

NASA ELECTRONIC PARTS & PACKAGING (NEPP) PROGRAM

EEE Links

March 2000, Vol. 6 No. 1

In this issue:

*Getters for Reliable
Hermetic Packages*



EPIMS 2.0



*Relay Failures
Specific to Space
Applications*



*Electronic-Discharge
(ESD) Failures in
Thin-Film Resistors*



*Nondestructive
Detection of Cracks
in Ceramics Using
Vicinal Illumination*



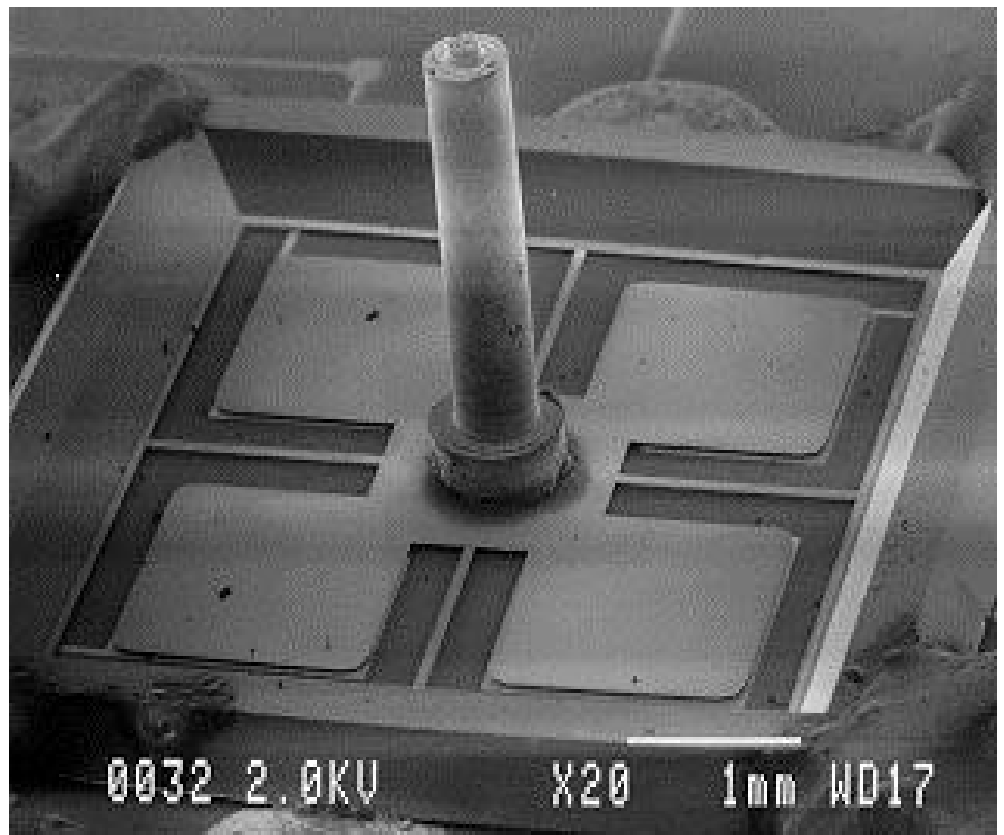
*Effects of Conformal
Coat on Tin Whisker
Growth*



*Evacuated FM08 Fuses
Carry a sustained Arc in
a Bus over 75 VDC*



*Status of Military
Specifications for Ceramic
Switch Mode Power Supply
(SMPS) Capacitors*



Editor: **Robert Humphrey, (301) 731-8625**

rhumphre@pop300.gsfc.nasa.gov

Mailing List Information and Article Submissions: (301) 731-8625

Desk Top Publisher: **Esther Bailey**

Published by the Information Management & Dissemination (IMD) Project

A Project of the NASA Electronic Parts & Packaging (NEPP) Program

http://nepp.nasa.gov/imd/eee_links

Table of Contents

Letter from the Editor.....	1
Getters for Reliable Hermetic Packages	1
Electronic Parts and Packaging for Space and Aeronautic Applications Advanced Technology Workshop (ATW).....	3
EPIMS 2.0.....	4
Relay Failures Specific to Space Applications	5
Electrostatic-Discharge (ESD) Failures in Thin-Film Resistors.....	6
Nondestructive Detection of Cracks in Ceramics Using Vicinal Illumination.....	13
Effects of Conformal Coat on Tin Whisker Growth.....	20
Status of Military Specifications for Ceramic Switch Mode Power Supply (SMPS) Capacitors	22
Evacuated FM08 Fuses Carry a Sustained Arc in a Bus over 75 VDC	23
Jet Propulsion Laboratory Parts Analyses	28
Goddard Space Flight Center Parts Analyses.....	28

Letter from the Editor

Robert Humphrey
 Editor of EEE Links
 (301) 731-8625
 rhumphre@pop300.gsfc.nasa.gov

Welcome to the March issue of EEE Links. As of October 1999, the EEE Links Newsletter is being published under the auspices of the NASA Electronic Parts and Packaging (NEPP) Program. The NEPP Program is responsible for performing technical assessments, characterizations, and evaluations of newly available and advanced (emerging) electronic parts and packaging, to enable their rapid infusion into NASA's hardware projects, thereby reducing the cost of mission success. These responsibilities all provide for a strong assurance function to develop and relate information regarding parts and packaging capabilities and limitations in order to assist NASA projects in decision making.

While serving the near-term needs of the NASA programs and projects, the NEPP Program also supports a core effort of longer range advanced technology evaluations that will expedite the readiness of the technology for commercial manufacture and project infusion. The NEPP Program provides an efficient manner for NASA to obtain electronic parts and packaging information and to sustain the availability of that information for broad usage across the Agency, industry, academia, and other government agencies. The NEPP Program provides a focus for and participation in Industry and Government Assurance Standards activities associated with electronic parts and packaging.

Keeping up with the latest technology advances has always been an extraordinary challenge. Remember EEE Links is one vehicle for sharing practical experiences and discoveries. Please keep us informed with your questions and needs so we can continue to improve the upcoming issues to meet your needs.

<http://nepp.nasa.gov>

Getters for Reliable Hermetic Packages

Rajeshuni Ramesham Ph.D.
 Applications Engineering Group, Quality Assurance Office
 Jet Propulsion Laboratory,
 California Institute of Technology
 4800 Oak Grove Drive, M/S 125-152, Pasadena, CA 91109

Executive Summary

A variety of sealed-off devices such as cathode ray tubes (CRT's), electron tubes, plasma displays, particle accelerators and colliders, vacuum thermal insulation, ultra-high vacuum (UHV), extreme high vacuum (XHV) systems for semiconductor processing, X-ray tubes, lamps, field-emission displays (FEDs), flat panel displays (FPDs), some microelectromechanical systems (MEMS) and science instruments for space applications nuclear systems require a vacuum for their successful operation. Maintaining vacuum in extremely small to large volume electronics hermetic packages and vacuum systems depends on the true surface area of the materials exposed to that volume as this is the source of species to be outgassed and it is this outgassing that will finally destroy the vacuum. Destroying the vacuum by outgassing from various materials used may lead to poor performance of the device (e.g., vibratory microgyroscope MEMS device). Getters are routinely used in small and large static systems and similarly getters will be needed if the desired system lifetimes of many years are to be obtained in MEMS and other packages for space applications.

JPL has been working on various types of microelectromechanical systems (MEMS) for space applications. Many high sensitivity microelectromechanical systems such as microgyros and some pressure sensors need to operate in hermetically sealed vacuum electronic packages to realize their full performance characteristics. This vacuum is destroyed by outgassing of various species such as water vapor, hydrogen, deuterium, tritium, methane, carbon monoxide, nitrogen, oxygen, methane, argon, nitrogen and carbon dioxide from the package surfaces and microleaking or permeation through the package body. The loss of vacuum is particularly serious if organic materials are used in isolated MEMS packaging device. A getter material is needed to eliminate this problem and to achieve successful MEMS device operation for long duration space applications. The

term “getter” refers to materials, which chemically sorb active gases in a vacuum environment. A solution is proposed using a nonevaporable high porosity getter material family such as the type of zirconium-aluminum-iron manufactured by SAES Getters Inc., to solve the hermetic sealing problem associated with the microgyro, other similar MEMS devices and other vacuum systems where hermetic sealing is required. The getter consists of a highly porous and mechanically stable packaging component installed inside the MEMS vacuum packaging chamber and subsequently activated.

The activation of the getter is a key step, which should be performed using a suitable combination of temperature and time. This removes the layer of surface oxides, nitrides, and carbides, by their diffusion into the bulk of the getter and provides a clean metallic surface ready to react with the impinging gaseous molecules in a vacuum environment. Depending on the diffusion constants for the elements (such as H₂, CO, CO₂, H₂O, etc..) into the getter materials, one can have a more or less effective cleaning of the surface during the activation process. The diffusion rate of various gaseous species present in the package increases upon raising the temperature of the getter material. The activation of the getter must be done when it is exposed for the first time or whenever exposed to air.

The solid-state getters may be either planar or three-dimensional and exhibit good mechanical strength. They must be particle free under the stringent operational conditions in space and on the ground, and they should have a high active surface area that can easily be activated at low temperatures. This minimizes problems such as high ambient temperature that may be detrimental to MEMS devices and other packages during the activation of getter. High porosity combined with a large active surface area of the nonevaporable getter will assure excellent sorption performances at room temperature. There should not be any loss of getter particles before, during, or after activation of the getter in a packaged MEMS device as this may cause failure of the MEMS device. It is critical to maintain the getter’s mechanical structure during shocks and vibrations at the time of spacecraft launch and during operation of the MEMS device. The presence of an activated getter material inside the MEMS package will allow achievement of a better

vacuum in the hermetically sealed vacuum package. The presence of a getter material inside a MEMS package is needed to avoid a pressure increase above the operational limit of the MEMS device. Sorption of outgassed species by getters permits a greater anticipated lifetime for MEMS devices in hermetically sealed packages.

I have provided an overview on various aspects such as gas sources in the electronics packaging, possible solutions, thermal treatment of packages, package materials, type of getters, applications of getters, preparation, characterization, and activation of getters, leak testing, and advantages and disadvantages of the various types of getters in various applications.

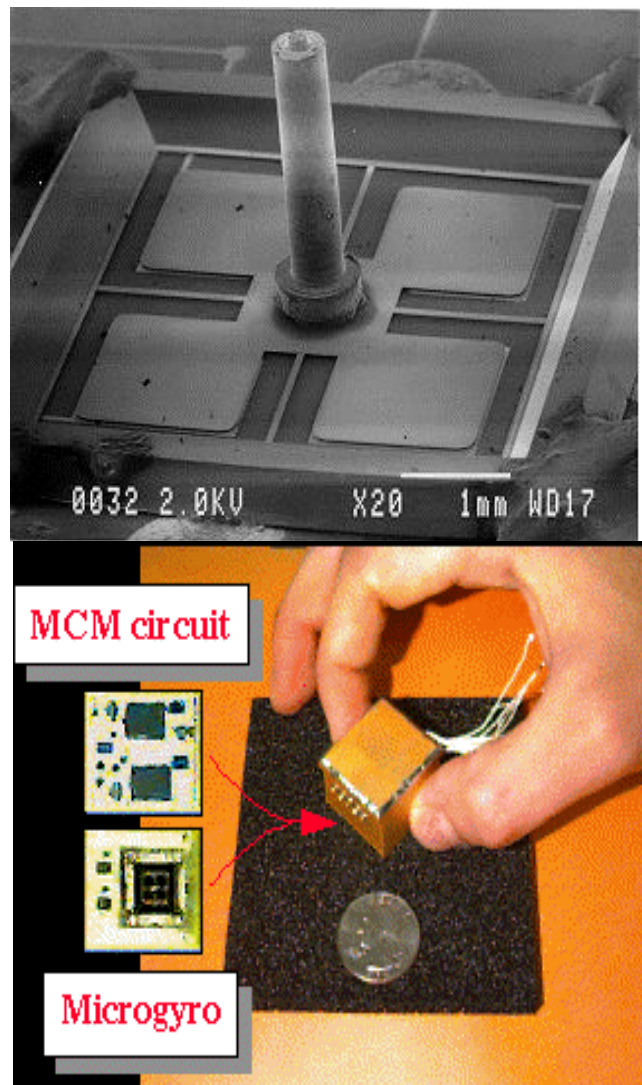


Figure 1. Packaging and Interconnect Development of JPL developed MEMS devices for Space Applications (Courtesy: Tony Tang, MDL/JPL)

This document will guide the researchers to select an appropriate getter for their respective application. The author of this document encourages the user to search for the latest information on this getter technology prior to implementing the concept of a getter to solve the problem in their specific application. (Total number of pages in the document: 88)

Acknowledgements: The document was put together at the Jet Propulsion Laboratory, California Institute of Technology, Pasadena, CA, under the contract with the National Aeronautics and Space Administration (NASA). It was primarily funded by the NASA Code Q under Research Technology Objectives and Plans (RTOP) and the Center Program Plan, UPN 100336-60.1 through Jet Propulsion Laboratory's Assurance Technology Program Office of Engineering Mission Assurance Division.

**Electronic Parts and Packaging
for Space and Aeronautic
Applications
Advanced Technology Workshop
(ATW)
to be held**

May 22-24, 2000 in Washington, D.C.

Lissa Galbraith
Jet Propulsion Laboratory
(818) 345-4617
Lissa.Galbraith@jpl.nasa.gov

Introduction

The NASA Electronic Parts and Packaging (NEPP) Program Information and Dissemination Project (IMD) is co-sponsoring an International Microelectronics and Packaging Society (IMAPS) ATW. The subject and title of the ATW will be "Electronic Parts and Packaging for Space and Aeronautic Applications".

Goal: to provide a forum for the exchange of information related to new and advanced electronic parts and packaging technologies for space and aeronautic applications.

Objectives

- Identify and explore trends in electronic parts and packaging for space and aeronautic applications in specific key technology areas.
- Promote the exchange of information between university, industry, government and NASA researchers.
- Foster an environment that stimulates discussions in potential technology partnerships and collaborations.
- Disseminate information about the NASA Electronic Parts and Packaging (NEPP) activities.

NEPP/IMAPS ATW Technical Program - Tentative

Monday, May 22

Registration

Opening Remarks

1:15 pm – 1:30pm

Lissa Galbraith, Jet Propulsion Laboratory, General Chair

Charles Barnes, Jet Propulsion Laboratory, NEPP Program

Phil Zulueta, Jet Propulsion Laboratory, Technical Chair

Session 1: Reliability of Electronics Under Extreme Environments

1:30 pm – 4:30 pm

Session Chair: Rajeshuni Ramesham, Jet Propulsion Laboratory

- Parts and Packaging for Low and High Temperatures
- Electronics Design for the Low Temperature Microgravity Physics Facility in the Space Station Environment
- Development and Application of High Temperature Sensors and Electronics Reliability of Integrated Passives on Flex Substrates
- At the NASA Glenn Research Center
- Reliability and Qualification of Electronics Systems at Elevated and Cold Temperatures

Session 2: Hi-Density Interconnect Microelectronics

6:00 pm – 9:00 pm

Session Chair: Reza Ghaffarian, Jet Propulsion Laboratory

- Copper Conductors in Space. Can We Trust Them?
- "System On A Chip" or "System In A Package" That Is The Question
- Recent Development in High Temperature Electronics and Sensor Packaging, and Wafer Scale Packaging for Microsystems
- 3D Packaging and Thin Package Technologies
- Effect of Underfill on CSP Reliability
- Reliability Evaluations for High I/O Ceramic Packages
- Thermomechanical Durability of High I/O BGAs

Tuesday, May 23**Session 3: MEMS and Sensors**

8:00 am – 11:30 pm

Session Chair: William "Bill" C. Tang, Defense Advanced Projects Agency (DARPA)

- MEMS Package Reliability Challenges
- Aero-MEMS Transducers: From Conceptual Design to Flight Tests
- High Performance Micromachined Microgyroscope for Space Applications
- Low Cost Vacuum Packaging for MEMS
- RF MEMS Relay and Tunable Capacitor
- MEMS Sensor Pressure Belt for Aircraft Flight Testing

Session 4: Radiation Characterization I

1:30 pm – 4:30 pm

Session Chair: Ken LaBel, Goddard Space Flight Center

- Overview of ERC Roadmap
- New and Existing Microelectronics Technologies
- Emerging Microelectronics Technologies
- Photonics (Optocouplers)
- Photonics (Transient predictions and fiber links)

Session 5: Radiation Characterization II

6:00 pm – 9:00 pm

Session Chair: Ken LaBel, Goddard Space Flight Center

- Flight Engineering Data Results
- High Energy Heavy Ion Facility

- Linear Device Hardness Assurance
- Terrestrial/Atmospheric Efforts
- Future Work: Advanced Sensors
- MPTB Results: Correlating Ground Tests to Flight

Wednesday, May 24**Session 5: Photonics/Optoelectronics**

8:00 am – 11:30 pm

Session Chair: Melanie Ott, Sigma Research and Engineering/Goddard Space Flight Center

- Space Qualification of Optoelectronic and Photonic Devices
- Kilowatt Peak Power Semiconductor Laser Arrays, The Challenge of Space Flight Qualification
- Characterization of Commercial Optical Fiber Cables for Space Flight Environments at NASA Goddard Space Flight Center
- Implementation of Optical Cables in a Spacecraft Environment.
- Root Cause of the Failure of Fiber Optic Cable on the International Space Station
- High Speed InP Based 1 x 2 Optical Switch

For more information contact General Chair

Lissa Galbraith, Ph.D lissa.galbraith@jpl.nasa.gov

Phone: (818)354-4617

EPIMS 2.0Stephen C. Waterbury
Code 562, NASA/GSFC

Component Technologies and Radiation Effects Branch

Phone: 301-286-7557

<http://epims.gsfc.nasa.gov>

Electronic Parts Information Management System (EPIMS) 2.0 has just been released. Some of the new features include:

- A new "Upload a Parts List" function, which provides the capability to upload parts lists via the user's Web browser and check them into the system (the user must have a "Project Data Administrator" role on a project ... see details below).
- An enhanced Parts/Components "Usage Search" functions, that now includes: a "Where-Used Summary", which reports all projects and design items in EPIMS that use any parts matching the search criteria.

- A "Manufacturer CAGE Summary", which provides a key with the names of all manufacturers whose CAGE codes appear in the search results.
- "Pop-up" kiosks to display summary information on vendors (by CAGE code), points of contact, parts lists, systems, and projects.

An Overview of EPIMS 2.0, including a synopsis of the current system functions, can be downloaded from: http://epims.gsfc.nasa.gov/epims_pub/epims_overview.pdf

There is a noticeable performance hit for the additional information that is gathered in the Part Usage search with Where-Used Summary -- typical search times are on the order of 20-30 seconds. This really isn't too bad when you consider the search is compiling the parts information from a database of over 250,000 parts in 6,819 parts lists, and the vendor CAGE information from a table containing over 750,000 CAGE codes.

For the "Upload a Parts List" function, additional access controls have been implemented to guard the system from unauthorized use. Please contact me if you need access to this function -- you will have to give me the numeric IP address of the workstation[s] from which you plan to upload parts lists, as access is controlled by IP address in addition to your user id, password, and role.

I am still working on the help documentation for that function -- what I have so far is at: http://epims.gsfc.nasa.gov/epims_pub/help/import_help.html

... but there are also lots of helpful notes displayed during the upload process.

With the release of EPIMS 2.0, the definitions of the user roles "Project User" and "Project Data Administrator" have changed somewhat: the Project User is allowed to add and modify Non-Standard Part Approval Request (NSPAR) data, but cannot upload parts lists. The Project Data Administrator role is required to upload project parts lists into EPIMS. For definitions of all EPIMS user roles, see: http://epims.gsfc.nasa.gov/epims_pub/help/person_role_help.html

(Note that there can be more than one Project Data Administrator on a project; also, any PDA can check-in a parts list for any item on their project[s], even if another PDA owned the previous version of that item's parts list ... this business rule may be subject to change based on user feedback -- right now it is geared toward simplicity and mutual benevolence among PDA's. Suggestions are welcome if there is a perceived need for more fine-grained control.).

Relay Failures Specific to Space Applications

Alexander Teverovsky
OSSMA GSFC/UNISYS
(301)-731-8690

Alexander.A.Teverovsky.1@gsfc.nasa.gov

Abstract

Low-pressure conditions, as experienced in space applications, are considered benign for many electronic components. However, for switching devices the probability of failure may be significantly greater than at normal atmospheric pressure due to arcing-at-break processes. This study was stimulated by a relay failure in a 60-V power bus in a spacecraft module, and it was intended to analyze failure modes and the probability of their occurring under low-pressure conditions. The effects of gas pressure, power bus voltage, and load current on arc duration and probability of arc flashover have been investigated. It was shown that arc duration mostly depends on switching power and gas pressure, significantly increasing when power is rising and pressure is decreasing. Failure analysis indicated two major mechanisms in low-pressure conditions: (1) contact damage (excessive erosion and/or microwelding) and (2) arc flashover to a grounded case and/or grounded coil post. For a relay operating in a vacuum, the effect of leak rate on the time to failure at low-pressure conditions is discussed.

Please contact the author for details of this investigation or see the entire paper in the Conference Proceedings from the 25th International Symposium for Testing and Failure Analysis (ISTFA) 1999 pages 285-292.

Electrostatic-Discharge (ESD) Failures in Thin-Film Resistors

Scott M. Hull
NASA/ Goddard Space Flight Center
(301) 286-4157
Scott.M.Hull.1@gsfc.nasa.gov

Abstract

Field failures of nichrome thin-film resistors have been investigated recently for several pieces of space-flight hardware. These failures have involved resistance shifts ranging from a few percent to complete open circuits. Failure analysis and duplication of these failures have revealed that the failures were caused by electrostatic discharge. The failure characteristics and the circuit conditions necessary for failure have been studied for several types of thin-film resistors, including nichrome and tantalum nitride resistive elements. The effects of latent damage and resistive pattern design will also be discussed.

Failure Analysis Experience¹

This investigation into the sensitivity of thin-film resistors to damage from electrostatic discharge (ESD) began as a result of a failure investigation². A hybrid electronic module for the Hubble Space Telescope gyro assembly failed during ground-level testing. The failure was isolated to a single 1500-ohm resistor within a thin-film resistor network chip, shown in Figure 1, that had developed an open circuit. This particular resistor had been connected between an isolated pin on the hybrid package and ground, and it was used as a precision reference resistor. Visual examination showed damage in the form of apparent cracks in the resistive film, in this case nichrome. These "cracks" (shown in Figure 2) were perpendicular to the major axis of the resistor and were crowded together in areas where the trace width was a minimum.

At first it was suspected that this damage resulted from some kind of over-power condition experienced during testing. Attempts to simulate this damage on spare resistor chips were unsuccessful, using both constant-power and pulse-power levels relevant to the

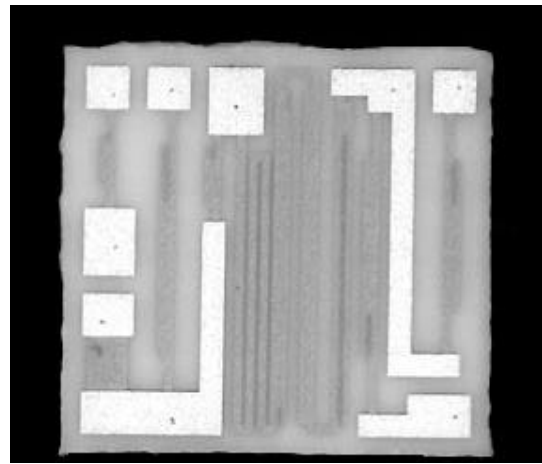


Figure 1. Overall view of the Hubble resistor network.



Figure 2. Close up vicinal view of the damage to the Hubble resistor.

application. Even excessively high power levels did not duplicate the observed effects. Test equipment designed to check for ESD sensitivity, however, produced the same kind of transverse, jagged, roughly parallel cracks as in the failed resistor. It was concluded that an ESD event had affected the Hubble hybrid. This was an unusual occurrence (the first of its kind that any of the analysts involved had experienced), so it was decided to investigate further and to determine the risk of further instances of this kind in other flight hardware.

Background and Literature Review

To facilitate better understanding of this phenomenon, a literature review was undertaken. Twenty-five articles were identified that might be of use in the investigation. Four of these articles were discounted

¹ M.J. Sampson, S. M. Hull, "Electrostatic Discharge Effects on Thin Film Resistors", CARTS '99, pp. 208-217 (1999)

² J. Slonaker, GSFC Failure Analysis Report Number EV88268 (1998)

because they dealt with different, but loosely related, subjects (for instance, a study of mechanical stresses induced during laser trimming). An additional five articles, which could not be located in several technical libraries, may be valuable to future studies^{3,4,5,6,7}.

A basic three-part tutorial, available over the Internet⁸, provides a good introduction to the sources, effects, and control of electrostatic discharge. Several articles were more directly applicable to the study of ESD effects on thin-film resistors. Among these, Lai⁹ and Chase¹⁰ have most closely duplicated the testing described in this paper. In both cases the authors used multiple ESD pulse sets to test tantalum nitride resistors. Lai tested capacitors and conductors in addition to resistors and described a method for calculating the temperature rise due to the ESD event. Chase used the Charged-Device Model (CDM), as well as the Human-Body Model (HBM), and confirmed the finding of the present study that a ground path is required for ESD-induced damage to occur.

A similar study by Ebel¹¹ examined the damage induced in cermet thick-film resistors. Several sources^{12,13,14} discuss the effects of ESD and electrical

overstress (EOS) on programmable read-only memory (PROM) fuses, which are similar to, but smaller than, typical thin-film resistors. A series of three papers^{15,16,17} by Wallash describes ESD damage on hard-disk read/record heads with a built-in air gap.

Several papers discuss the related physics and materials effects that occur during an ESD event on a thin-film resistor. For instance, Hagedorn and Hall¹⁸ have quantified the current crowding that occurs at sharp corners in resistive traces. Ramirez-Angulo et al^{19,20} have mathematically derived design rules for laser trim placement, size, and shape for highest resistance stability. Two additional papers^{21,22} discuss electromigration and vaporization at grain boundaries, which may help to explain the development of apparent cracks due to the ESD event.

It was noted that many of these papers had been published in journals and proceedings typically unfamiliar to the failure-analysis community. For that reason, this study, much of which has been previously reported¹, is being presented here.

³ V.D. Sadkov, D.E. Orlov, "Resistance of a Film Resistor with a Slit of Finite Width", *Radioelectronics and Communications Systems*, Vol. 35, Issue 11, pp. 62-64 (1992)

⁴ R.R. Avanesyan, Yu.P. Lazarev, A.N. Lugin, "Investigation of the Influence of Boundary Effects on the Stability and TCR of Thin-film Resistors", *Measurement Techniques*, Vol. 39, Issue 5, pp. 487-490 (1996)

⁵ J.F. Cain, L. Hart, J.R. McLean, "Failures in Thin Metal Film Resistors - A Case History", *Quality and Reliability Engineering International*, Vol. 8, Issue 2, pp. 99-104 (1992)

⁶ R. Veyhl, "Temperature Dependence of Thin-film Resistors", *CARTS-Europe '91*, pp. 110-114 (1991)

⁷ K.D. Robb, et al, "Analysis of Microstrip Resistors Using the Transmission Line Matrix (TLM) Method", *International Journal for Hybrid Microelectronics*, Vol. 14, Issue 2, pp. 62-69 (1991)

⁸ "Basics of Electrostatic Discharge", The ESD Association, <http://www.borg.com/~eosesd/cebasics.html> (1996)

⁹ T.T. Lai, "Electrostatic Discharge (ESD) Sensitivity of Thin-film Hybrid Passive Components", *Proceedings 39th Electronic Components Conference, IEEE*, pp. 229-239 (1989)

¹⁰ E.W. Chase, "Electrostatic Discharge (ESD) Damage Susceptibility of Thin Film Resistors and Capacitors", *EOS/ESD Proceedings*, pp.13-18 (1982)

¹¹ G.H. Ebel, "ESD Induced Failures in Cermet Trim Potentiometers", *ISTFA 1998*, pp. 139-142 (1998)

¹² D.M. Petkovic, "An Irreversible Resistance Transition in Polycrystalline Silicon Thin Film Resistors", *Vacuum*, Vol. 40, No.1/2, pp. 213-216 (1990)

¹³ J. Smith and W. Littau, "Prediction of Thin-film Resistor Burnout", *EOS/ESD Proceedings*, pp. 192-197 (1981)

¹⁴ R. A. Launer, J. T. May, L. M. Richard, "Interpretation of EOS Damage in NiCr Resistors", *ISTFA 1990*, pp. 279-284 (1990)

¹⁵ A. J. Wallash, "Electrostatic Modeling and ESD Damage of Magneto-resistive Sensors", *IEEE Transactions on Magnetics*, Vol. 32, Issue 1, pp. 49-53 (1996)

¹⁶ A.J. Wallash, T. S. Hughbanks, and S. H. Voldman, "ESD Failure Mechanisms of Inductive and Magneto-resistive Recording Heads", *EOS/ESD Proceedings*, pp. 322-330 (1995)

¹⁷ A.J. Wallash, M. Honda, "Field-induced Breakdown ESD Damage of Magneto-resistive Recording Heads", *EOS/ESD Symposium '97*, pp. 382-385 (1997)

¹⁸ F.B. Hagedorn and P.M. Hall, "Right Angle Bends in Thin Film Strip Conductors", *Journal of Applied Physics*, Vol. 34, No. 1, pp. 128-133 (1963)

¹⁹ J. Ramirez-Angulo, R. Wang, and R. Geiger, "Improvement of Laser Trimmed Film Resistor Stability by Selection of Optimal Trim Paths", *IEEE International Symposium on Circuits and Systems*, pp. 2188-2191 (1991)

²⁰ J. Ramirez-Angulo, R.L. Geiger, "New Laser-Trimmed Film Resistor Structures for Very High Stability Requirements", *IEEE Transactions on Electron Devices*, Vol. 35, No. 4, pp. 516-518 (1988)

²¹ A.J. Patrinos, J.A. Schwarz, "Simulation of Electromigration Based on Resistor Networks", *Journal of Applied Physics*, Vol. 75, Issue 11, pp. 7292-7298 (1994)

²² J.H. Linn, et al, "A Reliability Study of Laser Trimmed NiCr Kerfs", *41st Electronic Components and Technology Conference, IEEE*, pp. 883-889 (1991)

Further Characterization Study

PART DESCRIPTION

Parts used in this study were of two basic designs: pre-packaged resistor networks and single resistor chips that were custom packaged for electrical connectivity. These resistor networks were drawn from residual flight inventory to better represent actual parts used in NASA applications. All of the resistor networks contained nichrome patterns ranging from 625 to 25,000 ohms. Most of these patterns were complex serpentine traces, laser trimmed to the desired value. One of the networks was composed of eight rectangular blocks, each laser trimmed to form a simple serpentine pattern. The chip resistors were an assortment of simple blocks and serpentine patterns using either nichrome or tantalum nitride as the resistive material. Chip resistors ranged from 100 to 32,800 ohms.

TEST METHODS

ESD pulses were induced in the parts using an Oryx Technology System 700 commercial ESD tester. This tester is capable of delivering pulses from less than 100 to greater than 15,000 volts consistent with the HBM. The HBM, as opposed to the CDM or machine model (MM), is intended to simulate a pulse delivered by an ungrounded person (100 pF) discharging through skin (1500 ohms) into a grounded device. Many of the pulses were witnessed visually by placing the ESD tester under a stereomicroscope to facilitate observing the arcing location on a delidded device. A similar technique was used with an open shutter to photograph arcs in progress.

Visual inspection of the effects of ESD pulses was accomplished using a technique called vicinal illumination (described in more detail at this same conference). Standard lighting techniques typically fail to reveal ESD damage, or the damage is so subtle that it is difficult to study. Vicinal illumination is accomplished using a standard upright metallurgical microscope by closing the field diaphragm completely and maximizing the light output to produce a small bright spot near the center of the field of view. When that light is directed onto the substrate, it refracts into the substrate material and under the normally opaque resistive trace. If the resistive trace contains ESD

damage, the light is reflected through the "cracks" typical of ESD damage.

Scanning-electron microscope (SEM) inspection was used, but it was found to be totally ineffective for examining ESD damage in nichrome resistors. Tantalum nitride resistors, on the other hand, were examined quite successfully.

TEST TYPES

The basic test procedure was to measure the resistance of a trace, induce an ESD pulse, remeasure, and repeat with successively higher voltage pulses. The voltage starting point and increment were determined by first testing a sample resistor. It was understood that incremental ESD pulses impose a certain degree of error due to cumulative damage, but this was unavoidable because of the small quantity of parts available. Because of the sometimes subtle variations in the pattern shape or width, it was impossible to accurately estimate the effect of cumulative damage on the resistance measurements. When possible, however, an additional sample of a resistive path was given a single pulse at a voltage well above the damage threshold, and the resistance was measured. Usually these measurements fell either within the distribution for the sequential measurements or only slightly lower, so it is believed that the cumulative-damage effect was not major.

Another test was used to induce repeated pulses at the same voltage, with resistance measured after each pulse. To determine the effect of latent damage (a non-lethal ESD pulse that might get worse with use), several networks were exposed to various ESD voltages and then burned-in. The burn-in was 1000 hours at 105°C with cycled full rated power (50% duty cycle, 90-minute period). The resistance of each trace was measured at 0, 250, 500, and 1000 hours.

To facilitate better understanding of the ESD damage mechanism, glass slides were cut so that they just covered the resistive traces. Pulses were then imposed on the resistors with the slides in place in an effort to capture any material that might be vaporized by the ESD event and condensed on the cooler slide. The slides were then examined using an SEM with energy-dispersive spectroscopy (EDS) to determine the presence of evaporated nichrome.

RESULTS

There was a general trend among all samples that the damage threshold was proportional to the resistance of the trace being tested. As a rough rule of thumb, the damage threshold was approximately 1 volt/ohm. Multiple identical samples exhibited similar behavior, but the response was not perfectly predictable as shown in Figure 3. Initial intent was to measure physical dimensions of the resistor elements and attempt to relate these dimensions to ESD sensitivity. In fact, it was soon found that the simple effects of dimensional variation were overshadowed by the effects of configuration features in the resistor trace patterns, particularly serpentine and laser trims.

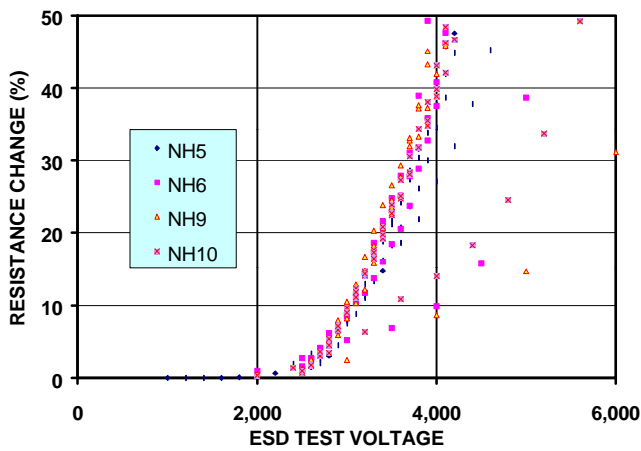


Figure 3. Typical reaction to ESD for nichrome resistors such as these 1250 ohm resistors

A polymer coating (assumed to be polyimide) on two of the test samples produced some interesting results. At low ESD voltage, the polymer apparently acted as an insulation blanket, preventing heat flow out of the resistor trace, especially in corners. As a result, these samples exhibited much heavier localized damage, wider cracks in the nichrome traces, and very predictable response as shown in Figure 4. At higher voltages, the coating apparently produced a carbon surface track during arcing events. Development of this stable arcing path protected the resistor from further degradation during repeated high-voltage ESD events.

A few resistors were exposed to repeated ESD pulses at the same voltage, with resistance measurements between pulses. Plots of these data (see Figure 5) show that the resistance increase was basically linear, with a slope proportional to the imposed ESD voltage.

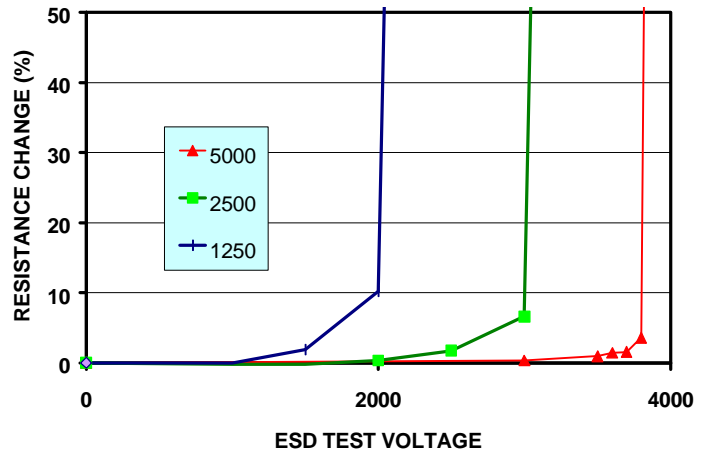


Figure 4. One pattern with polymer coating over the resistive elements showed this dramatic reaction to critical voltages.

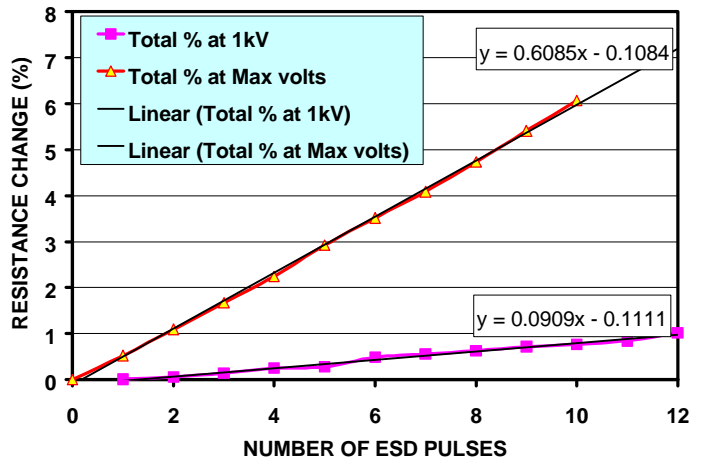


Figure 5. Pattern ND showed a linear reaction to repeated pulses at fixed voltages of 1kV and at 15.5kV

Extended pulses eventually resulted in catastrophic failure. Visual inspection between each pulse showed that the corner cracks grew steadily until the resistance of a serpentine trace had increased sufficiently to encourage internal arcing across the serpentine gap. Subsequent pulses produced continued arcing, eventually resulting in an open circuit and, usually, transverse cracks similar to the Hubble failure.

The tantalum nitride resistors tested to date have been simple block designs with “L-cut” laser trims. During the incremental voltage tests, voltage was ramped

from 100 to 15,500 volts in steps ranging from 100 to 1000 volts. In all cases, the resistance decreased after each pulse until approximately 3500 volts, at which point it increased rapidly. The maximum resistance changes measured were approximately 3.8 percent negative and 25 percent positive. Figure 6 shows the typical ESD-induced resistance decrease for a tantalum nitride resistor. One group of resistors was tested at opposite polarity, with close correlation of the parts within each test condition. Those tested with the high potential connected nearest the laser trim experienced larger resistance shifts (both positive and negative) than the resistors tested with the low potential near the laser trim. It is unclear what importance this may have, and further investigation is planned. Additional testing on tantalum nitride resistors in general is planned for the next phase of this study.

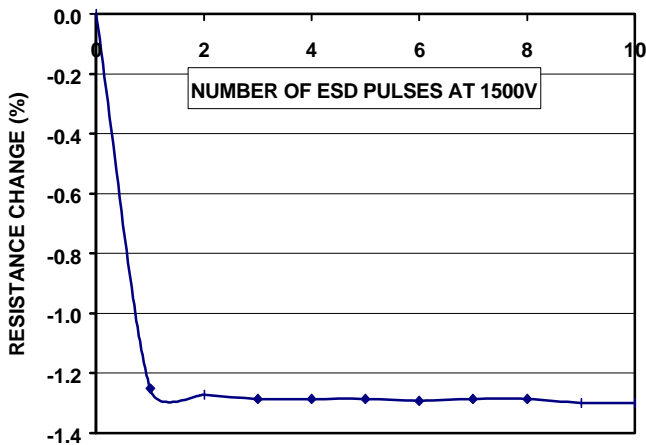


Figure 6. Significant resistance decrease exhibited by tantalum nitride pattern TF.

Discussion of Observations¹

Slope of the resistance versus imposed ESD voltage curve indicated four basic effects: little or no damage, current crowding, internal arcing, and external arcing. It should be noted that most of the resistive traces exhibited some, but rarely all, of these effects. For example, one sample exhibited only the “no effect” and “external arcing” effects due to the close spacing of the substrate bond pads. In another example, several traces in a network experienced no damage until

3000 volts, then exhibited external arcing at all voltages over 4000 volts (after the initial damage, however, the damage threshold decreased significantly).

“LITTLE OR NO EFFECT” REGION

Some resistors were visually inspected after each ESD pulse to establish a damage threshold below which no damage (typically corner cracking) was visible at 200X using vicinal illumination. The typical resistance-change (ΔR) threshold range for visible damage was 0.2 to 1.3 percent. Above this general range, the effects of current crowding were usually observed. The smallest values measured for ΔR were 0.01 percent.

“CURRENT CROWDING” REGION

The damage associated with the lowest voltage (and therefore lowest energy) pulses above the damage threshold involved the appearance of “cracks” in the resistive trace at corners and the tips of laser trims. These features resembled the branches of trees in that they split into numerous smaller paths as they developed at higher voltages. It is believed that these features were not actually cracks in the truest sense of the term because they were most likely thermally generated and not strictly mechanical in nature, but the term “crack” best describes their appearance. Vicinal-illumination inspection confirmed that the opaque resistive material was missing within these crack features. Their appearance and location suggest that the cracks result from higher current density around corners in the resistive trace (current crowding). Hagedorn and Hall¹⁸ have shown that the maximum current density in a right-angle turn with a radius of 1% of the trace width (a relatively sharp bend) is more than six times the current density in the straight portion of the resistive trace. Figures 7 and 8 show examples of corner-crowding-induced cracks. In some cases, cracks were observed across the entire width of the resistive trace, but often crack growth was suspended by the transition to internal or external arcing, which shunted the current, preventing it from flowing through the portions of the resistor that exhibited corner cracking. This transition was heavily influenced by the increase in resistance associated with the corner-cracking mechanism.

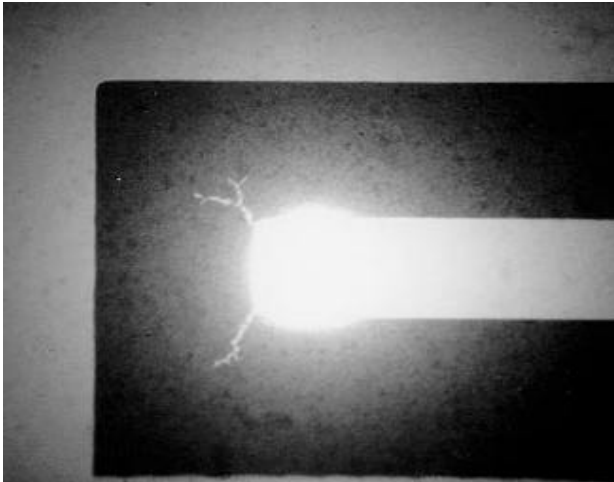


Figure 7. Vicinal illumination view of corner crowding induced damage.

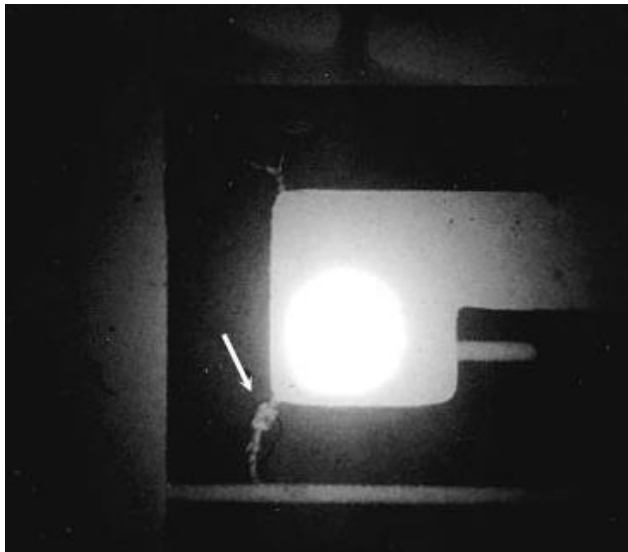


Figure 8. Typical corner crowding damage in a polymer coated resistor.

“INTERNAL ARCING” REGION

As the voltage (and therefore energy) of each ESD pulse was increased, eventually arcing would occur within the resistive pattern. Locations of such arcs varied from the base of the laser trim to gaps created by the serpentine pattern to high-potential-difference gaps created when the pattern doubled back on itself. The arcs tended to occur in as straight a line as possible between the substrate bond pads. In addition to

the resistance change evidence, vicinal-illumination inspection revealed a distinctive appearance for the damage resulting from internal arcing. The low-potential side of an arc always exhibited a branched crack structure extending into the trace from an edge, and the high-potential side exhibited only a few small chunks of nichrome missing from the edge of the trace. Examples of the damage caused by internal arcing are shown in Figures 9 and 10. During some



Figure 9. Vicinal illumination view of internal arcing damage.

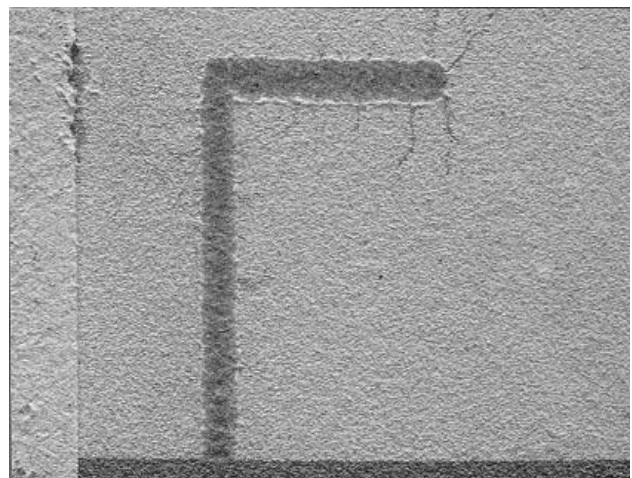


Figure 10. SEM view of ESD damage in a tantalum nitride resistor. Note the internal arcing damage to the left of the laser kerf.

what higher-voltage ESD pulses, arcs were observed directly using a stereomicroscope. Several of these arcs were photographed (see Figure 11), recording locations of the arcs. Internal arcing was often accompanied by the transverse cracks first observed in the Hubble failure (see Figure 12). It is believed that these cracks were the result of increased current density along thin areas of the nichrome, exacerbated by the low effective resistance experienced by the arc, producing higher current flow. At higher ESD voltages, external arcing tended to predominate.

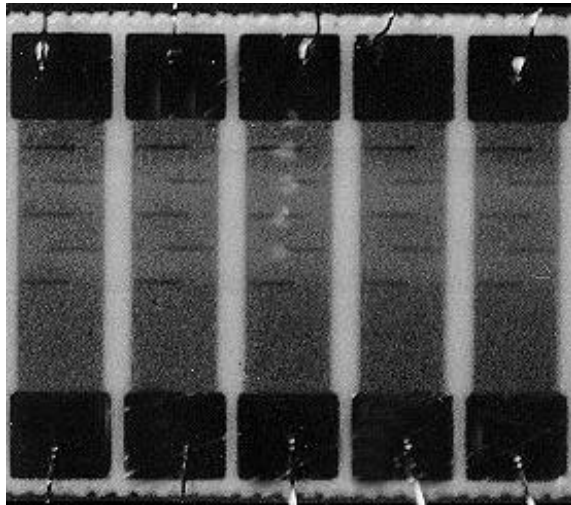


Figure 11. A photograph taken during an ESD induced arc event. Note the location of the arc on the center resistor.

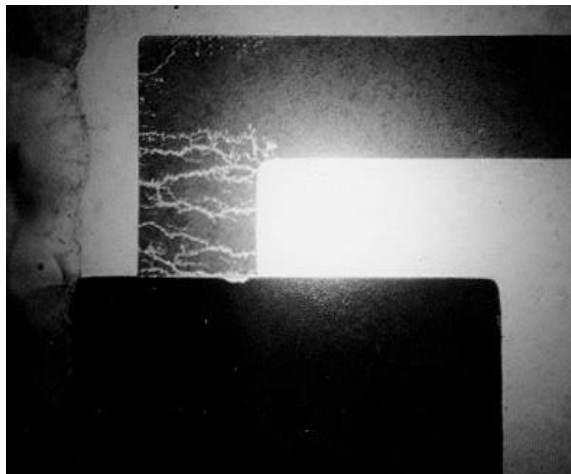


Figure 12. Vicinal illumination view of transverse cracking typical of relatively high voltage ESD damage.

“EXTERNAL ARCING” REGION

Many, but not all, resistor networks exhibited some degree of arcing outside the resistive trace. Potential locations of these arcs were between package bond pads, from package bond pads to substrate bond pads, between substrate bond pads, between adjacent resistors, and even between the bond pads and adjacent bond wires. External arcing usually shunted all of the current flow around the resistive element, but in some cases resistance continued to change despite external arcing, indicating that some amount of current flow was causing damage to the remaining resistive material. External arcing was typically easy to observe using the stereomicroscope described above, and it was observed that the location often shifted slightly from one ESD pulse to the next. Visual inspection at higher magnification revealed that external arcing typically resulted in metal deposition near the low-potential side of the arc and a melted appearance on the surface of the high-potential side of the arc.

Presence of a direct ground connection at one end of the resistor was required in all cases to produce ESD damage. Several resistors were tested without a ground connection to the subject resistor or an adjacent trace, and in no such case was any damage observed, either electrically or visually. This finding, confirmed by Chase¹⁰, is significant because it helps to explain why ESD failures are not more common in thin-film resistors. Consider, for example, the case of a discrete packaged resistor network; damage to any individual resistor in it would be extremely unlikely given that an ESD pulse would have to be delivered while the pin connected to the other end of the resistor (typically an adjacent lead) was connected to ground potential. This requirement for a ground suggests that thin-film resistors are much more susceptible to ESD damage after being installed into larger assemblies that have their own ground connection. This was the precise situation for the Hubble failure, which was found during board-level testing.

Future Work¹

As is so often the case, this investigation seems to have raised more questions than it answered. The surprising result that tantalum nitride resistors can show negative resistance changes in reaction to ESD should be investigated. Is this behavior dependent on

the manufacturer's processing? Does it happen with serpentine as well as block patterns? Plans are in place to procure both block and serpentine pattern tantalum nitride resistors from a different manufacturer in addition to performing further testing on the present samples.

During brief experiments with changes in polarity on tantalum nitride samples, some interesting effects that should be further investigated were observed. Similar testing should also be performed with nichrome resistors to determine whether the previously noted difference between the two systems extends to polarity sensitivity as well.

From the work described in this paper, it has been postulated that rounding the insides of serpentine bends will reduce current density and thus increase robustness, but this hypothesis was not tested. Samples with radiused bends will be tested in the next phase of work.

Conclusions

1. Thin-film resistors made from both tantalum nitride and nichrome are ESD sensitive.
2. Locations and shapes of damaged areas can be used as failure-analysis guides for estimating the magnitude and polarity of an ESD insult.
3. Sensitivity levels of the resistor patterns tested in this investigation were influenced by many unexpected factors in addition to, or instead of, simply the width, length, thickness, and resistivity of the resistance trace.
4. Too close spacing of the pads of separate resistors can lead to unexpected damage, caused by the ESD pulse jumping to the adjacent resistor.
5. ESD damage to nichrome resistors can be expected to increase resistance, whereas tantalum nitride resistors may decrease in resistance when subjected to relatively low-voltage pulses.
6. Characteristics of the damage are fairly predictable depending on the form of the resistor trace; serpentine patterns tend to show damage on the inside radii of the bends, laser scribes show arc damage, etc.
7. Dimensions and locations of laser trims can significantly impact ESD sensitivity of thin-film resistors.
8. Some of the ESD damage characteristics are sensitive to the polarity of the applied charge.
9. In practice, ESD damage to thin-film resistors is probably quite rare due to the requirement for a charged surface at one end and a grounded surface at the opposite end of a resistor trace.
10. ESD damage to thin-film nichrome resistors appears to be stable as the part is operated.

Acknowledgements

The authors wish to thank the following people who supported this work: Andre Pelham and Prashant Patel, the high-school students who performed most of the ESD testing; Doug Macpherson of Electrofilms, Inc. and Fred Castello of Teledyne Electronic Technology, who provided some of the test samples and considerable knowledge and experience, and the management of the National Aeronautics and Space Administration for vital resources and the opportunity to perform the experiment.

Nondestructive Detection of Cracks in Ceramics Using Vicinal Illumination

Scott Hull

NASA / Goddard Space Flight Center
(301) 286-4157

Scott.M.Hull.1@gsfc.nasa.gov

ABSTRACT

Cracks and other defects in ceramic materials can be difficult or impossible to examine and photograph due to the extreme lack of contrast. A method for inspecting translucent ceramics using scattered light, also known as vicinal illumination, will be described. This method has been known in the ceramics industry for quite some time, but is not well known in the testing and failure analysis community. Electronics applications include substrates, packages, multilayer capacitors, and thin film resistors.

Ceramic materials are used in electronic applications as microcircuit packages and substrates which carry signals and power between microcircuits. Fine cracks in ceramic materials can result in mechanical failures, electrical failures, and loss of hermeticity. Often, fine cracks are difficult or impossible to detect using standard nondestructive inspection techniques such as visual inspection, ultrasonic inspection, or vapor crack detection. Dye penetrant inspection is usually effective, but contaminates the part, which is unacceptable for space flight hardware.

One effective nondestructive inspection method of detecting cracks involves examining the way in which light scatters through the ceramic material when viewed with a standard bright field reflected light microscope. This method, termed vicinal illumination, has been used for detecting cracks during failure analyses of several part types, and screening of space flight hardware. The technique has proven effective on several different types of ceramic materials as well. A related method for use with dark field equipment has also been used to successfully locate otherwise invisible cracks.

INTRODUCTION

Cracks in ceramic devices can cause degradation of their performance, or even catastrophic failure in some applications. Nearly invisible microcracks can propagate under stress, resulting in mechanical failure. For this reason, in critical applications it is imperative that such cracks be detected prior to use. Several techniques are available to locate and characterize cracks in ceramic materials. Each has advantages and limitations which can affect the choice of the optimum inspection method for a given application.

Visual examination is usually performed on ceramic materials at some time during their manufacture or use. A large crack which significantly displaces the surface of the part will probably be detected at that time. Visual inspection is fast and inexpensive, but small cracks may go undetected. One way to enhance visual inspection is to spray a relatively expensive inert fluorocarbon vapor over the ceramic surface. The fluorocarbon seeps into any cracks in the surface, and retains a shiny appearance after the remainder of the fluorocarbon evaporates. This method is capable of pointing out small cracks more effectively than a simple visual inspection, but requires a skilled operator to interpret the various defect indications.

A similar technique uses a dye to penetrate into cracks and clearly indicate their location. Dyes are available which are visible using either white or ultraviolet light. Dye penetrant inspection is among the most effective and widely used techniques for detecting cracks, but it requires that the part be contaminated with a dye which may not be entirely removed.

X-ray radiography and acoustic microscopy have also been suggested as crack detection methods for ceramic materials. Radiography is not successful for crack detection unless the crack is parallel to the x-rays, and exhibits an appreciable gap. Since this is not usually the case for cracks in ceramics, this method is rarely useful. Acoustic microscopy (also known as ultrasonic inspection or C-SAM) has been used to detect known cracks in laboratory samples with some success. This method, however, is limited by the necessity of immersing the part in water and by the rather time consuming inspection process. A crack could also be overlooked easily using acoustic microscopy, due to difficult gating issues and spurious signals from echoes in the part.

One effective non-invasive method of optical crack detection involves introducing light into the sample and observing the way in which the light scatters through the ceramic material. Ceramicists have reportedly used this technique to observe cracks in research samples for many years²³, but the technique is not widely used in testing and failure analysis. The technique has been referred to as "vicinal illumination" because the sample is illuminated near, but not directly onto the area of interest.²⁴ Because it is totally nondestructive, this method can be used for screening, quality control, and failure analysis. The technique is nearly as fast as visual inspection, and requires little or no sample preparation. Operators can be taught to perform this technique in minutes using a standard bright field microscope. The main limitation to the usefulness of the light scattering inspection method is that the material must be inherently translucent.

In vicinal illumination, light is refracted into the sample in a small area, and scatters outward in all directions. If the light encounters a crack, the majority is reflected back toward the source, and very little is transmitted across the crack. This causes a high contrast delineation between bright and dark areas at a crack surface.

²³ M.J. Viens, Effect of microstructure on impact damage of polycrystalline alumina, University of Massachusetts, Master of Science thesis (1986).

²⁴ V. Freschette, Personal conversation, New York College of Ceramics (1993).

MATERIAL PROPERTIES

Light scattering inspection has been used successfully on several different types of translucent materials. The important factor is the ability of the material to scatter light uniformly. As a rule of thumb, vicinal illumination inspection can be performed successfully on materials similar to a business card in translucence. Grain size, material composition, additives, porosity, and surface finish all can affect the light scattering ability of the material.

Quantifying this property is difficult, since no standard measures of light scattering or translucency of ceramic materials seems readily available.^{1,25} In an attempt to quantify the differences between the light scattering capacity of different materials, the percent transmission of white light through samples of different materials was measured. From this data and the sample thickness, an absorption coefficient can be computed for each material using the formula:

$$\ln(I/I_0) = -\alpha\chi$$

where I/I_0 is the ratio of light transmitted through the sample, χ is the sample thickness, and α is the absorption coefficient.

The light transmission properties of several samples of typical ceramic materials were measured using a visible light 630 nm laser and a power meter. The results are shown in Table 1. The lack of homogeneity in the samples and the effect of thickness is clear from these measurements. For instance, the measurements for aluminum oxide varied inversely with sample thickness. It is believed that thinner samples exhibited more internal reflection, scattering the light further from the source, outside the power meter window area. The inherent material properties such as grain size and density also induced some variation in the data.

In general, light scattering inspection is successful for materials with an absorption coefficient of 40 to 200. In the case of a transparent material, light is transmitted through the material, and is not refracted sufficiently to scatter to the sides. Dark field light scattering works well for the more transparent mate-

rials (absorption coefficient of approximately 50 to 100). Bright field inspection can be used with the more transparent materials as well, but the dark field technique is preferred due to simpler setup and faster inspection. Materials with an absorption coefficient of 100 to 200 are best inspected using the bright field technique. An opaque material such as a business card reflects and absorbs the light as it enters the material, preventing it from scattering.

Table 1. Absorption Coefficient for Several Ceramic Materials

Material	Thickness	α (inch ⁻¹)	Preferred Vicinal Inspection Method
Glass Slide	0.038	2	Not Applicable to Transparent Samples
Aluminum Nitride	0.054	73	Dark Field
Aluminum Nitride	.104	45	Dark Field
Aluminum Nitride	.107	56	Dark Field
Aluminum Oxide 96%	0.025	167	Bright Field
Aluminum Oxide 99.5%	0.026	182	Bright Field
Aluminum Oxide 96%	0.042	121	Bright Field
Aluminum Oxide 96%	0.122	51	Bright Field
Business Card	0.011	535	Not Applicable to Opaque Samples

The thickness of the ceramic part also contributes to the amount of light available for inspection. Light scattered through a relatively thin sample is reflected by the back surface, resulting in increased brightness on the sample surface. Scattered light would tend to be hemispherical in a thicker sample, resulting in less usable light for crack detection. It is important to note, however, that there is sufficient light for vicinal illumination to be effective for bulk samples so long as a crack is open to the surface of the material.

INSPECTION APPLICATIONS

Light scattering inspection was most successful for white aluminum oxide electronic substrates and packages. Unfortunately, most ceramic electronic packages are made with black or purple colored materials. Additives in these materials cause them to be more opaque, and therefore difficult samples for light scattering crack detection. One of the case histories involves such a material, however.

This technique was also used to locate cracks in an aluminum nitride plate which was designed as the base of a multichip module package. Vicinal illumination also has revealed cracks in beryllium oxide

²⁵ L.H. VanVlack, "Physical Ceramics for Engineers", Addison-Wesley, Reading, MA, p. 207 (1964)

substrates used in high power electronic devices. In addition, a porous silicon dioxide glass substrate used in a large charge coupled device had the ability to scatter light due to internal reflections off the voids within the material.

Vicinal illumination has been used by other investigators to confirm the location of cracks in BaTiO₃ multilayer capacitors.²⁶ This technique has been used on capacitors for failure analysis, and also as a screening technique for cracks in the cover plates. Inspection of cracks in capacitors is most successful following metallography. The conductor plates in the capacitor act as mirrors to extend the useful inspection distance laterally.

A recent application of vicinal illumination is the detection of electrostatic discharge (ESD) damage in thin film resistors. Scattered light travels through a ceramic substrate beneath the opaque resistive trace. If the trace contains ESD damage, the light shines up through the lightning-like damage path showing the absence of resistive material.

MICROSCOPE SETUP

For the purposes of this paper, there are two basic types of reflected light microscopes; bright field and dark field. A stereo microscope that would be used for a typical low magnification visual examination uses dark field lighting to produce an image. Light is reflected off the surface of the sample from some angle other than perpendicular, and travels through the objective to the eyepieces. Dark field microscopes are often equipped with external light sources which can be positioned at any angle.

Bright field reflected light microscopy (also known as coaxial or epi illumination) requires that the light be introduced from an internal light source through a beam splitter so that the light strikes the sample normal to the surface being examined. Most bright field microscopes contain two diaphragms used mainly to reduce glare in the image. Because of their different locations in the light path, the effect of each is unique. The aperture diaphragm controls the amount of light entering the back focal plane of the objective. Closing the aperture diaphragm excessively re-

sults in a darker image and decreased resolution. The field diaphragm is located such that it is focused at the sample plane. Closing the field diaphragm results in a small roughly circular area of light near the center of the field of view. It is the field diaphragm that creates the small spot of light used for vicinal illumination inspection.

PROCEDURE

Bright field crack inspection is performed by opening the aperture diaphragm fully to maximize the light input, and closing the field diaphragm fully to create a small spot of light. Any filters between the light source and the sample should be removed if possible. Inspection can be performed using any magnification, but a 10X objective with 10X eyepieces (final magnification of 100X) seems to be the best general starting point. The sample should be brought into focus and examined in the field of view **outside** the bright area. Magnification up to 500X can be used to further refine the beam size and placement relative to a suspected crack.

The sample should be examined around the entire perimeter, watching for an abrupt line of high contrast. As the sample is moved so that the light spot traverses the crack, the bright and dark areas should exchange places. It should be noted that any opaque metallization on the surface of the sample may alter the light path, and could be mistaken for a crack. Also, it can be helpful to displace the field diaphragm to the edge of the field of view, if the microscope has such an adjustment.

Dark field inspection is performed in a similar manner, but requires a more transparent sample. A high intensity concentrated light source (a fiber optic gooseneck lamp, for instance) should be positioned close to the sample, nearly perpendicular to the surface. Examination is performed using a typical low magnification (10X to 120X) stereo inspection microscope. Because dark field inspection can be performed at lower magnification, it is usually faster than the bright field technique for inspecting large samples. As with the bright field method, abrupt bright and dark contrast indicates the presence of a crack.

²⁶ D. Johnson-Walls, M.D. Drory, A.G. Evans, D.B. Marshall, and K.T. Faber, Evaluation of the Reliability of Brittle Components by Thermal Stress Testing, Journal of the American Ceramic Society, Vol. 68, No. 7 (1985)

CASE HISTORIES

THIN FILM SUBSTRATE (FIGURES 1,2)²⁷

Electrical testing of a high frequency amplifier for use on the TOPEX satellite revealed that several thin film microwave substrates had cracked during mounting into the chassis. A nondestructive method of screening was required to ensure that the remainder of the substrates in the chassis did not contain any latent defects. Standard visual inspection was not considered reliable, and the use of dye penetrant would have contaminated the space flight hardware. A bright field microscope was fitted with a long working distance lens from a macro camera for the inspection. A video camera and large screen television were added to reduce eye strain and allow several people to inspect the samples simultaneously. Each of approximately one hundred substrates was inspected around the perimeter, and through the center of the substrate. No additional cracks were observed in electrically functional areas, and the amplifier was flown with a high level of confidence. This amplifier is still in operation today.

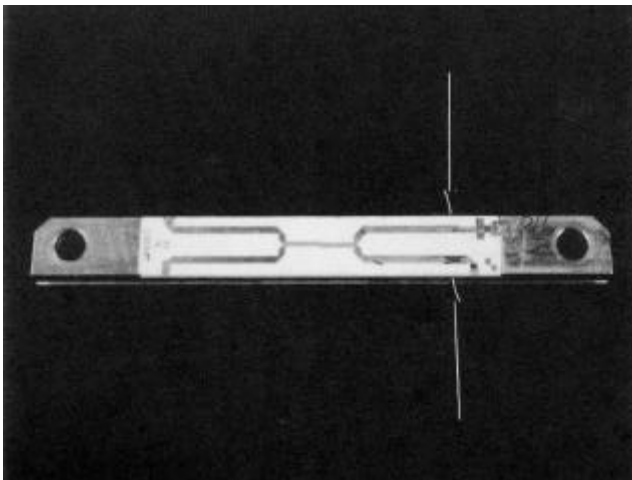


Figure 1. An overall view of a cracked amplifier substrate.

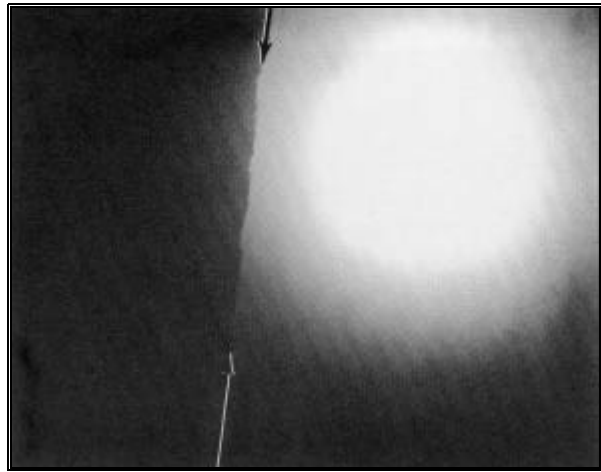


Figure 2. A vicinal illumination close-up view of the crack indicated by the arrows.

ALUMINA PACKAGE (FIGURES 3,4)²⁸

A hybrid microcircuit used in the POLAR spacecraft failed electrically during testing. The package, which was made from thick film substrate material, was inspected using bright field light scattering, which revealed a crack across one corner. This technique was also able to show the shape of the crack. From this information the crack initiation site was traced to one of the package leads. It was subsequently discovered that moisture leaking through the crack had caused dendritic growth within the package, leading to the electrical failure. This failure was associated with a lack of hermeticity in the ceramic package.

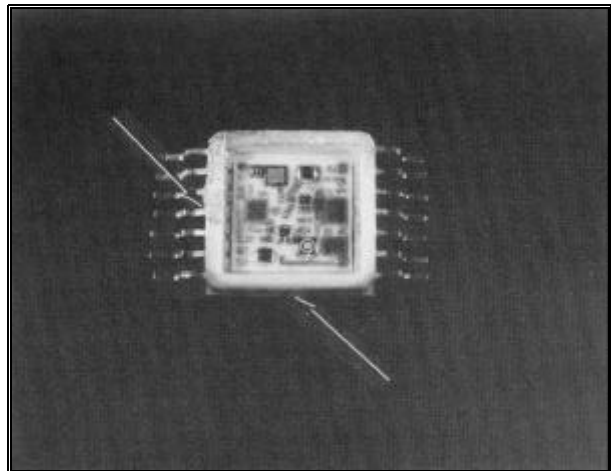


Figure 3. An overall view of the hybrid package.

²⁷ S. Hull and J. Evans, NASA Goddard Space Flight Center Parts Analysis Laboratory, FA00257, Greenbelt, MD (1990).

²⁸ P.O'Shea, NASA Goddard Space Flight Center Parts Analysis Laboratory, FA31448, Greenbelt, MD (1993).

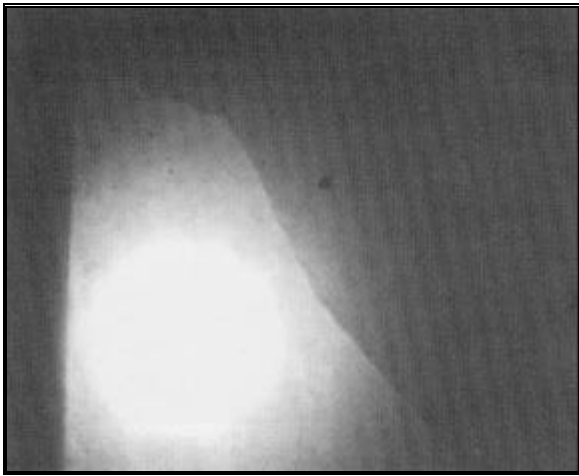


Figure 4. A vicinal illumination close-up view of the crack which resulted in a leak path. Vicinal illumination was used to trace this crack across the entire corner of the package.

MULTICHIP MODULE (FIGURES 5,6)

Bright field inspection of a multichip module showed a small chip-out in one corner of an alumina substrate. The chip-out seemed to be isolated from any electrical circuitry, and not a reliability risk. Vicinal illumination, however, revealed a crack extending from the chip-out toward an electrical connection, which could eventually result in device failure during use. The existence of this crack underscores the need for careful handling and inspection during the processing of advanced components.

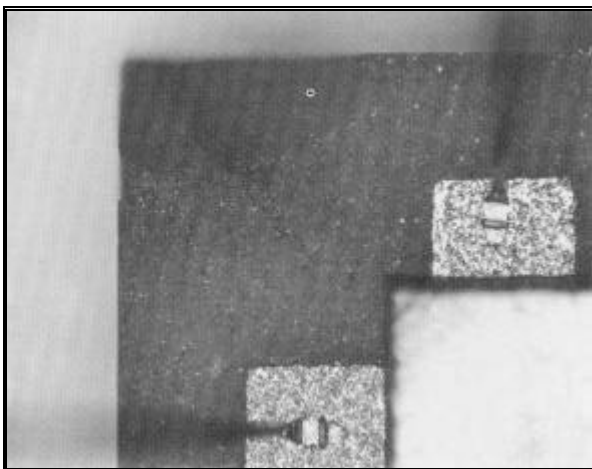


Figure 5. An overall view) of a chip-out in a multichip module.

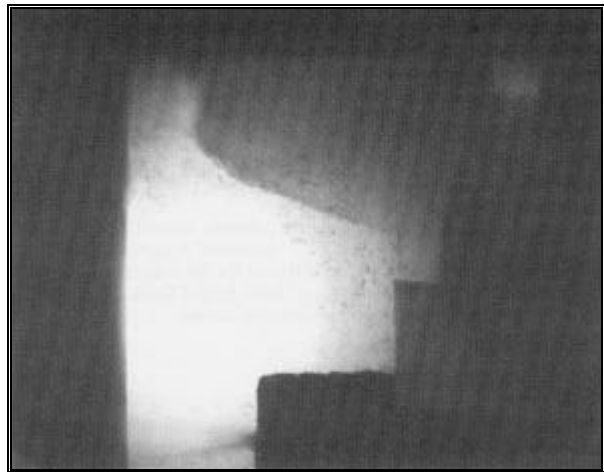


Figure 6. A vicinal illumination view of the same area. Vicinal illumination revealed a crack extending from the chip-out toward active circuit metallization.

ALUMINUM NITRIDE SUBSTRATE (FIGURE 7)

Several five inch square aluminum nitride substrates were evaluated to determine their suitability for use in multichip module packages for space flight use. Throughout the evaluation, dark field light scattering inspection was used to determine the mechanical integrity of the samples. Following a thermal cycling test, one chip-out and several secondary cracks were observed in one corner. During subsequent tests, the status of the cracks was closely examined, and no further crack propagation was observed.

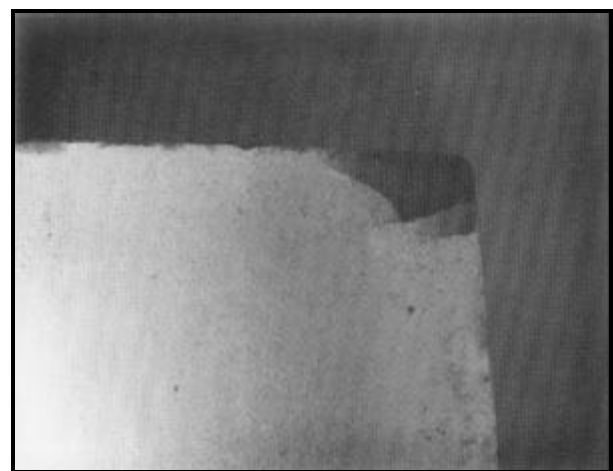


Figure 7. Dark field light scattering photograph showing damage to the corner of an aluminum nitride substrate.

**MULTILAYER CERAMIC CAPACITOR
(FIGURES 8,9)**

Multilayer ceramic chip capacitors are prone to fracture during manufacture and also during soldering operations. When such a fracture occurs across opposite plates a current leakage path can be formed, resulting in unacceptable electrical performance. The two cracks shown in this example are currently benign since one crack extends through the cover plates to a single conductor plate and the other extends through two common conductor plates. Such cracks can, however, develop into moisture leakage paths or catastrophic mechanical failures.

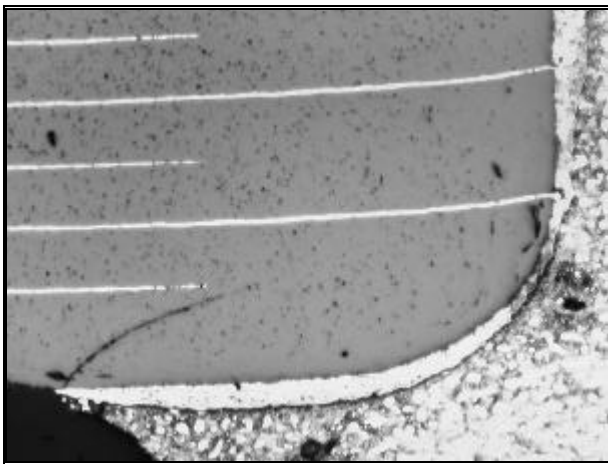


Figure 8. Bright field view of a multilayer ceramic capacitor.

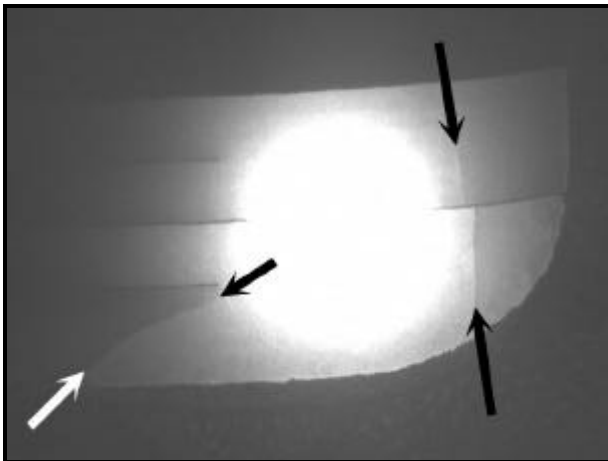


Figure 9. Vicinal illumination view of the same capacitor. Note the crack to the right of the light spot which was revealed only using vicinal illumination.

**THIN FILM RESISTOR ESD DAMAGE
(FIGURES 10,11)**

An investigation of an open circuit failure in a hybrid for the Hubble Space Telescope indicated that the resistor had failed as a result of electrostatic discharge (ESD) damage. A study was then conducted to determine the pertinent design characteristics for ESD susceptibility. In the course of this study many resistor networks using different patterns, materials, and resistance values were intentionally exposed to ESD pulses. The vicinal illumination technique was used to examine each resistor and determine the location and nature of the effect on the resistive elements. The examples shown include high voltage transverse cracks, corner cracking, and internal arcing over laser kerfs.

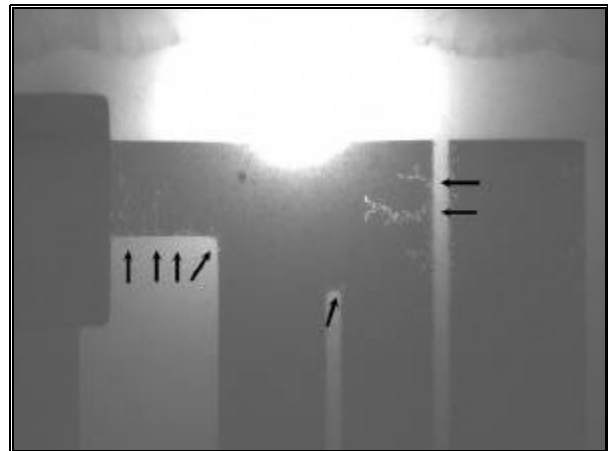


Figure 10. Vicinal illumination photograph showing electrostatic discharge damage on a thin film nichrome resistor within a resistor network.

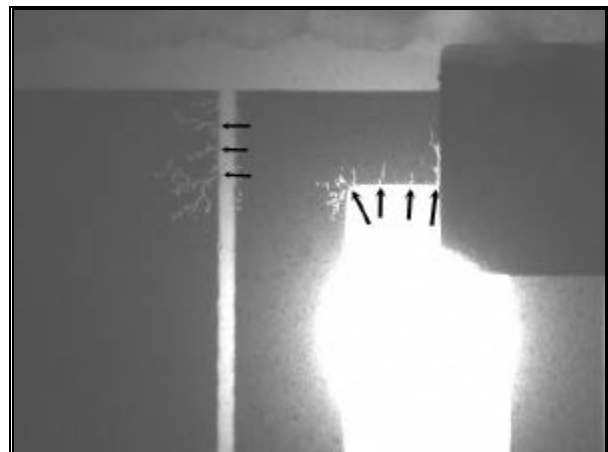


Figure 11. Vicinal illumination photograph showing electrostatic discharge damage on a thin film nichrome resistor within a resistor network. This damage was completely invisible using standard lighting.

CONCLUSION

The vicinal illumination technique has been successfully used to detect cracks in many types of ceramic materials. The effect of inherent material properties on the suitability of the technique has been studied and discussed. Several case histories have shown the efficiency and effectiveness of both bright field and dark field techniques used for failure analysis, screening, and routine evaluation. This inspection method has become an important tool for inspection and analysis of many ceramic materials for space flight applications.

Effects of Conformal Coat on Tin Whisker Growth

Jong S. Kadesch
Unisys/NASA
e-mail: jkadesch@pop300.gsfc.nasa.gov
301-286-2785

This article provides a status report on an experiment to study the effects of a conformal coat on tin whisker growth initiated by NASA Goddard 13 months ago. Interim updates have been reported and documented on a regular basis on the Code 562 web site:

<http://nepp.nasa.gov/whisker/>

Tin whisker formation from pure tin plated surfaces is well known and documented. However, little research has been conducted to understand the benefits (if any) of using protective barriers such as conformal coat to prevent whisker formation or to inhibit growth. Although NASA prohibits the use of pure tin plating, there is still a possibility that some devices may still contain pure tin plated surfaces (i.e., Commercial Off-The-Shelf Components (COTS), hybrids, etc.). The presence of conformal coating is often used to mitigate the whisker concern. In these situations, projects need to understand the risks of continued use and potential benefits of using a protective coating over the tin surface.

Most published literature on tin whiskers agree that brass with a bright tin finish is a combination that promotes whisker formation. Whether conformal coating could provide enough protection against whisker growth is unknown and the literature search regarding the conformal coating associated with tin whiskers was unsuccessful. Therefore the experiment was dedicated to understanding the role of the conformal coating on tin whisker growth.

For this experiment several brass substrates (some with copper flash) have been plated using a "bright" tin finish. The literature suggests that the bright tin plating process is most susceptible to whisker formation due to residual stresses in the surface material. Introduction of scratches in the surface also creates localized stresses that may promote whisker formation. To further promote whisker formation some of the plated samples were scratched using a knife blade.

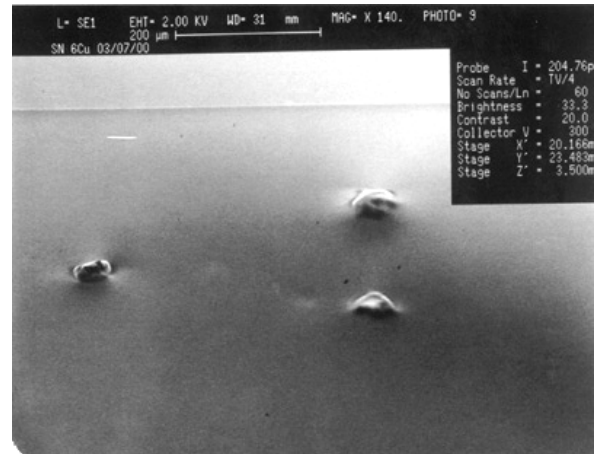
The samples were segregated into two test groups. Portions of each sample were coated with Uralane 5750 conformal coat material. Uralane 5750 was selected because of its widespread use in NASA systems. One test group has been placed in an oven at 50 °C because the literature suggests that whisker growth is greatest at this temperature. The other test group is being stored at room temperature. All samples are being visually examined periodically to determine;

- If conformal coat inhibits whisker formation
- If whiskers are capable of growing outward through the conformal coat
- Incubation period for whisker formation
- Rate of whisker growth

The latest observation indicates that tin whiskers under the conformal coat are pushing their way outward causing dome shapes in the coating. As time progresses, these dome shapes become larger and narrower at the top, which suggests that the whisker tips are beginning to penetrate the tough skin of the conformal coat. Figure 1A and 1B show whiskers at the same location taken a year apart. Similarly, Figures 2A and 2B are SEM photos taken at another site six months apart.



A. Picture taken on 3/11/99



B. Picture taken on 3/15/00

Figure 1. Whiskers forming under coating



A. Picture taken on 8/5/99



B. Picture taken on 3/15/00

Figure 2. Whiskers forming under coating

Among 14 samples, only 3 samples show these dome shapes. Two of these samples are kept at room temperature; one is copper flashed and the other is pure tin over a brass metal substrate. Figure 3 shows whiskers from a bare metal surface, without coating, and some whiskers are growing a lot faster than others. This one particular whisker is estimated to be 0.8 mm in length. This is, of course, relatively small to cause any short circuits. However, other experimenters have recorded tin whiskers on the order of 1 cm or more.



Figure3. Whiskers from uncoated side

Some general observations from our experiment to date include:

- Even though complete penetration of whiskers through coating is not yet observed, it is definite that the coating is slowing down the whisker growth.
- Despite of the optimal temperature for tin whisker growth at 50 °C, there are more whiskers and taller whiskers from the samples that are kept in room temperature.

The experiment is ongoing. Please visit our web site for further updates. This work is being done under the guidance of Dr. Henning Leidecker (NASA GSFC) with significant technical assistance provided by Scott Kniffin (Unisys Corporation).

Status of Military Specifications for Ceramic Switch Mode Power Supply (SMPS) Capacitors

Jay Brusse
 Unisys Corporation at NASA Goddard
 (301) 286-2019
 Jay.A.Brusse.1@gsfc.nasa.gov

The US Military, NASA and the manufacturing community have worked diligently over the last few years to develop a Military procurement specification for ceramic Switch Mode Power Supply (SMPS) capacitors. This specification known as MIL-PRF-49470 [Capacitor, Fixed, Ceramic Dielectric, Switch Mode Power Supply (General Purpose and Temperature Stable), General Specification for] is accessible from the Defense Supply Center Columbus (DSCC) web site at:

http://www.dscccols.com/offices/doc_control/

MIL-PRF-49470 is intended to replace the DSCC drawing for similar capacitors, DSCC-DWG-87106. To date, two suppliers (AVX Olean Advanced Products and Presidio Components) have qualified a small portion of the available capacitance/voltage ratings available. Users are encouraged to start using the MIL-PRF-49470 parts in lieu of the DSCC drawing as soon as qualified sources become available.

Procuring parts through MIL-PRF-49470 instead of DSCC-DWG-87106 will provide users with a more

reliable part. Some of the advantages of MIL-PRF-49470 over DSCC-DWG-87106 are:

Requirement	MIL-PRF-49470	DSCC-DWG-87106
Formal Qualification Process (QPL Established)	Yes	No
MIL-STD-790 Compliance	Yes	No
DSCC Audits	Yes	No
Routine Qualification Maintenance Testing (i.e., Life Testing)	Yes	No
Group A Percent Defective Allowed (PDA) Specified	Yes	No
Prohibits Mixing of Chips from Different Production Lots within a Single SMPS Stack Lot	Yes	No

DSCC’s plan is to:

- Inactivate DSCC-DWG-87106 parts for new design when one supplier qualifies for the equivalent MIL-PRF-49470 part
- Cancel DSCC-DWG-87106 in its entirety when all parts on the drawing have two qualified sources for the equivalent MIL-PRF-49470 parts.

The QPL for MIL-PRF-49470 is available for download at DSCC's website.

http://www.dscccols.com/offices/sourcing_and_qualification/

As products are qualified, the associated MIL-PRF-49470 capacitors will be added to the NASA Parts Selection List www site at: <http://nepp.nasa.gov/npsl>

Recently, MIL-PRF-49470 was modified to include a "space level" product. However, at the time of this article, no sources have attained qualification for space level product. Some of the key additional requirements for the space level product include:

- Non-destructive internal examination (acoustic microscopy or other means)
- Chip Level DPA/Stack level DPA
- Humidity, Steady State, Low Voltage
- Extended Voltage Conditioning
- Lot Sample Thermal Shock plus Life Testing on all Lots

Evacuated FM08 Fuses Carry a Sustained Arc in a Bus over 75 VDC

H. Leidecker

NASA/Goddard Space Flight Center

J. Slonaker

Unisys/NASA GSFC Operations, Lanham, MD

ABSTRACT

The FM08 style fuse is specified to interrupt an overcurrent of up to 300 A in a bus of up to 125 VDC, but this applies only when its barrel is filled with air. When placed into a space-grade vacuum, the FM08 style fuse exhausts its air within a year. Then, the probability of an enduring arc is high for all ratings when the bus is above 75 VDC, and the overcurrent is large. The arc endures until something else interrupts the current. The fuse can violently eject metal vapor or other material during the sustained arcing.

The evacuated FM08 does not develop a sustained arc when interrupted in a bus of 38 VDC or less, at least when there is little inductance in the circuit. This is consistent with its successful use in many spacecraft having buses in the range 24 to 36 volts.

INTRODUCTION

The FM08 style fuse is widely used throughout the spacecraft industry. For example, there are several hundred on a typical National Aeronautics and Space Administration (NASA), Goddard Space Flight Center (GSFC) spacecraft, and there are almost a thousand on the Hubble Space Telescope. GSFC uses these fuses almost without exception in buses of nominally 28 VDC, for which the usual range is 24 to 32 VDC, with a few reaching 36 VDC. For this range of bus voltages, these fuses satisfactorily interrupt overcurrents even after many years in space.

Military standards and specifications do not address all applications in all situations. For example, the FM08 is defined by MIL-PRF-23419/8, which speaks only to behaviors in air; behaviors in a vacuum environment are not mentioned [1]. The space community has known since about 1970 that it is necessary to derate the current ratings of the FM08 series in order to obtain adequate mission lifetimes, especially after the fuse exhausts its internal air into a space-level vacuum.

At the beginning of this decade, Mr. Richard A. Williams demonstrated that depressurizing a fuse of conventional design (a wire filament contained within a normally air-filled barrel) could lead to sustained arcing. He patented an alternate design [2], and described in the "prior art" section the enduring arc he observed upon overcurrenting an evacuated 10 A conventional fuse with a 17 A current in a bus of 100 VDC. He did not report his observations except in this patent, and they did not become widely known.

There are two published studies [3,4] of enduring arcs that form when a tin whisker is shorted across 50 VDC at pressures less than 0.5 torr. In atmospheric air, tin whiskers fuse open at a current of a few milliamperes; however, at sufficiently reduced pressures, the puff of tin vapor is ionized into a plasma that evolves into an enduring arc carrying a current of hundreds of amperes. Circumstances had acquainted us with the details of this work [5]. Thus, when we were asked by the Canadian Space Agency in January 1999 whether the FM08 style fuse might develop an arc after becoming evacuated and then subjected to an overcurrent in the International Space Station (which uses a nominally 125 VDC bus), we responded that this was likely. We then demonstrated that sustained arcs did happen at this bus voltage for fuses evacuated to 1.0 torr, at least at large overcurrents, and published NASA Parts Advisory NA-045 (March 1999).

We carried out a second series of tests that showed that the threshold voltage for arcing was in the neighborhood of 60 to 75 VDC for fuses evacuated to 1.0 torr, at least for large overcurrents.

The purpose of this paper is to describe these ongoing series of tests. The goal is to characterize the FM08 style fuse well enough to evaluate the risk (if any) when using it in busses with voltages higher than the traditional (nominal) 28 VDC.

PARTS DESCRIPTION

Aspects of the construction of the FM08 style fuse and its behaviors are specified in MIL-PRF-23419/8. The FM08 is a fast acting, compact fuse rated for use in buses up to 125 VDC, except for the 15 A current rating which is rated for use in buses up to 32 VDC. These ratings apply only when the fuse is used in air. The FM08 is comprised of a metal filament passed

through a ceramic body tube (4.8 mm long, 0.68 mm inside diameter) and wrapped around each end of the tube, with a short overhang. An end cap lead assembly (a copper lead butt-welded to a brass end cap) with a solder preform is slid over the end of the tube, trapping the wrapped-around end of the filament. The preform is melted, soldering the filament to the end cap. This ensures an electrical connection between the lead and the filament, and it weakly seals the end cap to the tube's end. Then the assembly process is repeated at the other end. A sleeve made of irradiated polyvinylidene fluoride (Kynar®) is slipped over the fuse, extending slightly beyond each end-cap. The sleeve is heated, which shrinks it tightly around the barrel and end caps, creating a seal that has sometimes been called "hermetic," and adding mechanical support in the axial direction. See Figure 1 for a drawing of the construction of the fuse. Each candidate for FM08 status has the leak rate of this seal checked by a hot oil immersion test; however, this only demonstrates that the leak rate is below about 10^{-5} atm-cc/s [6]. The volume of the barrel's cavity is 0.0015 cc, and a leak rate of less than 1.6×10^{-11} atm-cc/s is needed to maintain the cavity's pressure above 1 torr for twenty years (a desirable design life for the fuse) in a space-vacuum environment. Analysis of the failure of three FM08 fuses used on the Solar Maximum Mission, launched in 1980, indicate that each of these fuses leaked down to a cavity pressure of some 0.1 torr in nine to ten months, implying a leak rate of $(5.1 \text{ to } 5.7) \times 10^{-10}$ atm-cc/s.

The material of the filament is not specified directly; however, conformance with the specified cold and hot resistances and with the specified interruption times constrains the material. The filament material is pure nickel for current ratings between 1/8 A and 1/2 A; an alloy of copper and silver (50% by weight) for ratings between 3/4 A and 4 A, and pure copper with a silver jacket for ratings between 5 A and 15 A. Only the filament changes as the current rating changes (except that the diameter of the leads attached to the 10 A and 15 A ratings are larger).

Item	Item Name	Material
1	Outer Sleeve	Polyvinylidene fluoride modified by radiation
2	Barrel	Ceramic (MIL-I-10, Grade L3B)
3	Filament Wire	Ni for 1/2A and below, Cu/Ag alloy 3/4to 4 A Cu, Ag coating above 5A
4	End Cap	9010 brass alloy Au plated
5	Lead	Soft copper, Au plated
6	Solder	98% Sn, 2 % Ag (232 °C)

Figure 1. Schematic drawing of an FM08 fuse. The numbered items are described above.

EXPERIMENTAL PROCEDURE

We obtained FM08 fuses from space flight residuals and the commercial version of FM04 (series 275) for the testing. The FM04 style is identical in construction to the FM08 fuse except that the external leads have tin plating instead of gold plating. The specifications provide for upgrading the FM04 to FM08 status when a subplot passes the extra tests called out in MIL-PRF-23419/8. This had been done for some of the specimens we used.

Each fuse in the experiment was serialized and the cold resistance at 22 to 24 °C was measured using Kelvin-style connections: the uncertainty was typically less than 0.04 mΩ. A small hole was cut through the Kynar sleeve and the ceramic body tube using a diamond saw, so that the interior of the fuse would quickly equilibrate to the pressure of a test chamber. (We note that this also allows material to escape rapidly during arcing, and thus limits the internal pressure built up by the arcing. In a later series of tests, we will seal the venting hole after the fuse's barrel has been evacuated, and before arcing.) The cold resistance was remeasured and compared to the earlier values. Any fuse whose cold resistance changed by more than 3% was removed based on probable damage induced during cutting. However, a notch cut halfway through the filament of a 15 A fuse would increase the cold resistance by only 1%; the increase is less for fuses with smaller current ratings. Using a 30 X microscope, the filament was inspected through the hole and no blade markings were noted on any of the several dozens inspected.

The fuses were placed one at a time into a chamber whose pressure could be brought to any measured

pressure down to 0.5 torr. Current was provided by a stack of car batteries (each nominally 12.4 V), a bounceless switch (mercury wetted power relay), a protection fuse (30 A slow blow ATO fuse;

$I^2 \cdot t = 1050 \text{ A}^2 \cdot \text{s}$), a 5.00 m Ω current shunt, an adjustable carbon stack power resistor, and a fuse holder. Short straight lengths of heavy gauge wire were used to minimize stray inductance (measured to be less than 10 mH) and excessive resistance. The total resistance of the circuit, exclusive of the resistance of the fuse, is called the ballast resistance; it can be adjusted to be as low as 0.10 Ω . The voltage across the fuse, the voltage drop across the shunt resistor, and the voltage delivered by an active clip-on current probe were monitored using a digital oscilloscope. The equivalent circuit is shown in Figure 2.

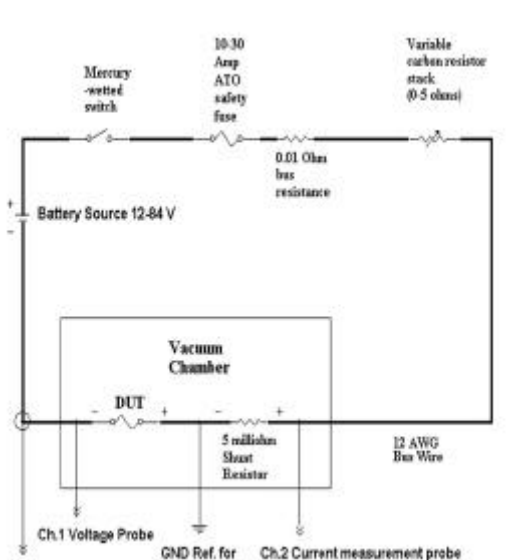


Figure 2. Electrical schematic of the test station used to overcurrent the fuses.

The ballast resistance was set (using the adjustable carbon stack power resistor) so that the maximum current was 100 A, simulating a dead-shortened fuse. The actual current flowing through the fuse before its filament melted depended on the current rating of the fuse and on the voltage chosen for the run, and was sometimes much lower than 100 A. For example, the cold resistance of a 1/8 A fuse is $2.1 \Omega \pm 10\%$ and its hot resistance is $8.0 \Omega \pm 15\%$. Therefore, at 37.3 volts (three batteries), the maximum current available is 17 A at the start of the overcurrent, dropping to less than 4.6 A as the filament melts, when the ballast resistance is set to its minimum value of 0.10 Ω .

The intent is to simulate a “hard short circuit” interruption within a space system. However, our present choice is not as severe as MIL-PRF-23419 specifies for the FM08 style fuse: it is specified to interrupt 300 A at 125 VDC without developing a sustained arc, without rupturing its case or spreading debris or vapor, and without restriking; further, the post-interruption resistance must exceed 10,000 Ω .

The chamber that contained the fuse and current shunt was pumped down to a pressure of 1.0 to 1.5 torr. Throwing the bounceless switch started the test. This switch also triggered the storage oscilloscope, recording the voltage across the fuse, the voltage across the current shunt and the voltage from the current probe. A digital record was made of each run. Ten specimens were destructively tested at each voltage level.

RESULTS AND DISCUSSION

During a normal event, a fuse will interrupt the current flow within the time listed in the MIL-PRF-23419. This event was viewed as clearing by having the fuse filament heat, melt, and then vaporize in its normal time period. Normally, when overcurrent interrupts the fuse filament, an arc is formed during the vaporization of the filament, but is suppressed by the surrounding air that absorbs the heat of the arc and quenches it very rapidly. In a sustained arc situation, the arc is launched from the cathode end during the vaporization of the filament like that in the normal clearing event, however the arc remains. This arc produces and sustains a hot metal vapor plasma that increases with size as it consumes the surrounding metal. Several physical factors known to control arc formation are available voltage, internal pressure, ballast resistance, inductance, and ambient temperature.

There is always a spark whenever two current-carrying contacts are separated in a bus exceeding 10 to 12 volts. This happens in a circuit breaker, or a relay, or a power switch, or the separating parts of the filament of a fuse. The designer works to ensure that the duration of this spark is not so long that the power that is let through the device interferes with its use. Other things being equal, the duration of the spark increases with the bus voltage, until a point is reached when the cathode develops “cathode spots,” each able to supply a current of roughly a hundred amperes so

long as bus voltage is supplied and suitable material remains at the cathode: this is a sustained arc [7,8,9].

For each of the fuses we studied, the overcurrent and the pre-arcing time for the filament to separate are related by “ $I^2 \cdot t = \text{constant}$ ”; the value of the constant depends on the rating, and is known to within about 25% for each rating of the FM08 style fuses. See Table 1. Any test for which the observed $I^2 \cdot t$ value exceeds the tabled value is carrying overcurrent for a prolonged time, and the excess amount of $I^2 \cdot t$ is a direct measure of the extra energy let through. However, we are most interested in those cases in which the arcing endures until some other component interrupts the current. Then, the energy let through can reach enormous values, limited only by the robustness of the other circuit components and not by the fuse. Further, the internal arc can rupture the case of the fuse and broadcast debris and soot.

Rated Current (A)	$R_{\text{cold}} \pm 10\%$ (mΩ)	$I^2 \cdot t$ (A ² ·sec)
1/8	2100	7.93×10^{-4}
1/4	710	7.84×10^{-3}
3/8	420	2.12×10^{-2}
1/2	280	4.62×10^{-2}
3/4	170	2.12×10^{-2}
2	55.0	0.361
4	23.0	2.30
5	14.0	4.90
7	10.0	11.0
10	6.5	24.6
15	4.0	60.6

Table 1. Values of the cold resistance, and values of $I^2 \cdot t$ that produce a normal interruption by melting.

The voltage and current traces were used to classify each run as “no sustained arc” or as “sustained arc”. See Table 2. Inspection shows that the probability of a sustained arc is zero for a bus voltage of 37.3 VDC. The probability of a sustained arc is high as the bus voltage exceeds 75.0 VDC. For intermediate bus voltages, the probability scatters, and a dependence on the current rating of the fuse is apparent; still, a probability for sustained arcing of even 10% is unacceptably high for spacecraft use and this happens for the 7 A rated fuse for buses as low as 50 V.

The metal filament of the FM08 is so small, for most ratings, that the air within the barrel is enough to absorb the heat of the spark, and quench it so rapidly that there is negligible energy let through. The exception is the 15 A rating: the specification only rates this example for use in a bus of 32 VDC. The filament of this rating is large enough that internal air at a nominal one atmosphere (760 torr) is not enough to quench the spark excited by buses at above 32 VDC and below the 125 VDC rating. In previous experiments, using a 300A overcurrent value at 1 torr pressure, it was found that three out four 15 A fuses sustained an arc using 49.7 V (4 batteries). It is no surprise that reducing this air pressure, already inadequate at 760 torr, down to the region of 1 torr, would still not quench the spark supported by this quantity of metal vapor.

Rating (A)	37.3 V (3 bat)	49.7 V (4 bat)	62.0 V (5 bat)	74.4 V (6 bat)	86.8 V (7 bat)
	Number of fuses that had a sustained arc in a sample of 10				
1/8	0	0	1	8	9
1/4	0	0	0	9	NT
3/8	0	0	0	4	5
1/2	NT	NT	0	9	10
3/4	NT	0	0	7	3
2	NT	NT	NT	1	3
4	NT	0	5	5	6
5	NT	0	2	2	8
7	0	1	0	1	4
10	0	0	0	5	4
15	0	0	0	1	8

NT = Not tested

Table 2. Results of the overcurrent testing.

CONCLUSION AND RECOMMENDATIONS

A soft vacuum environment (1.0 to 1.5 torr) within the FM08 style fuses has been shown to cause a sustained arc within the fuse at bus voltages of 50 VDC and above. Under a high current short situation, where a fuse could go into a sustained arc mode, damage to the fuse and surrounding mounting is probable. More importantly, the fuse will not protect the power system as intended. For many designs, the next upstream fuse will interrupt, isolating systems that

should still be allowed to be powered. This problem will propagate further if the same arcing happens in that next upstream fuse. Typically, in space systems, reliability is sought from redundancy: a failed unit is cut off the bus and a working one is substituted. This approach fails when one or more fuses develop a sustained arc, rather than interrupting per design intent, upon experiencing an overcurrent.

We believe that the successful operation of the FM08 style of fuse in GSFC spacecraft has been dependent on the use of a nominal 28 VDC bus, with the tacit voltage derating by a factor of more than four from the specified 125 VDC. Our intentions are to extend the derating criteria at GSFC for the use of this style of fuse to include the need for a voltage derating, as well as the current derating already in use.

More testing at other overcurrents, other barrel pressures, and other ambient temperatures is needed. In addition, conditions affecting "restrike" potential, including the role of inductance in the circuit, are needed.

ACKNOWLEDGMENT

This work has been supported by the Parts Branch at the Goddard Space Flight Center in Greenbelt Maryland. The authors appreciate the valuable assistance of Mr. Prashant Patel in the testing laboratory, and conversations with the manufacturers of this type fuse. The authors thank Mr. Rodney Woolley (Canadian Space Agency) for bringing this problem to our attention, for pointing out Mr. Williams' patent, and for many useful discussions.

REFERENCES

- [1] MIL-PRF-23419, Military standard for fuses. See also slash sheets MIL-PRF-23419 /8, /4, and /11.
- [2] Patent US5446436: "High voltage high power arc suppressing fuse"; Inventor: Mr. Richard A. Williams (Palo Alto, CA); Applicant: Space Systems/Loral, Inc. (Palo Alto, CA); Issued Aug. 29, 1995. Abstract: A high voltage high power fuse for use in a low pressure environment such as space.
- [3] J. H. Richardson, and B. R. Lasley, "Tin Whisker Initiated Vacuum Metal Arcing in Spacecraft Electronics," 1992 Government Microcircuit Applications Conference, Vol. XVIII, pp. 119 - 122, November 10 - 12, 1992.
- [4] D. H. Van Westerhuyzen, P. G. Backes, J. F. Linder, S. C. Merrell and R. L. Poeschel, "Tin Whisker Induced Failure in Vacuum," 18th International Symposium for Testing & Failure Analysis, pp.407 - 412, October 17, 1992.
- [5] <http://misspiggy.gsfc.nasa.gov/whisker/>
- [6] MIL-STD-202, Method 112A, Condition A. (Seal testing)
- [7] Max F. Hoyaux, *Arc Physics*, Springer-Verlag, 1968
- [8] *Handbook of Vacuum Arc Science and Technology* edited by Raymond L. Boxman, D. M. Sanders, P. J. Martin. Noyes Publications, New Jersey, 1995.
- [9] *Circuit interruption: theory and techniques*, Edited by Thomas E. Browne, Jr. Marcel Dekker, Inc., New York and Basel, 1984.

Jet Propulsion Laboratory Parts Analyses

Joan Westgate
NASA/JPL
818-354-9529
joan.c.westgate@jpl.nasa.gov

Failure analyses (FA), destructive physical analyses (DPA) and part construction analyses (PCA) have been performed on the following part types. For a copy of the report, contact me (phone 818-354-9529, fax 818-393-4559 or e-mail to joan.c.westgate@jpl.nasa.gov) and request the desired document by "Log#".

NOTE: THE SUBJECT JPL REPORTS MAY CONTAIN PROPRIETARY INFORMATION
WHICH IS SUBJECT TO LEGAL RESTRICTIONS. QUESTIONS REGARDING THIS NOTICE
SHOULD BE ADDRESSED TO JOAN C. WESTGATE.

FAILURE ANALYSIS				
Log No.	Manufacturer	Date Code	Part Type	Part Number
8236	Sprague	9415	Resistor, 5.11K Ohm	RM1005
DESTRUCTIVE PHYSICAL ANALYSIS				
Log No.	Manufacturer	Date Code	Part Type	Part Number
8240	DIT	Unknown	Chip Capacitor, 470 pF	N471K0544X*K
8254	AKO	-	Chip Capacitor, 0.01 μ F	O504BD103CP
8255	AVX	9930	Chip Capacitor, 0.1 μ F	O9075C104KAKIA
8253	AKO	-	Chip Capacitor, 0.001 μ F	O504BD102CP
8258	AKO	-	Chip Capacitor, 3.3 pF	O504BD3R3CP
8239	DIT	Unknown	Chip Capacitor, 3300 pF	N332K0544X*K
8238	DIT	Unknown	Chip Capacitor, 4.2 pF	N42DK0544X*K
PART CONSTRUCTION ANALYSIS				
Log No.	Manufacturer	Date Code	Part Type	Part Number
8156	Lockheed Martin	9837	ASIC Column Grid Array	M1132

Goddard Space Flight Center Parts Analyses

Listed below are the EEE parts analyses completed by the GSFC Parts Analysis Laboratory. The GSFC reports are available to NASA personnel and current NASA contractors by contacting your NASA project office.

CA JOBS						
Job Number	Manufacturer	Date Code	Part Type	Part Number	Result	Date
99418	DALE	9805	FILTER	WSL-2010	P	12/04/99
EV JOBS						
Job Number	Manufacturer	Date Code	Part Type	Part Number	Result	Date
08851	CERAMIC	UNKN	CAPACITOR	VARIOUS	P	11/22/99
90505	ATC	9901, 9750, 9745	CAPACITOR	CDR12BGXXXKJUS	P	11/01/99
99696	MICROSEMI CORPORATION	9601, 8950	DIODE	JANTXV1N5811	P	10/12/99
99696	MICROSEMI	9601	DIODE	JANTXV1N5811	P	10/12/99

FA JOBS						
Job Number	Manufacturer	Date Code	Part Type	Part Number	Result	Date
99789	INTERPOINT	9846, T9809	HYBRID	5962-9316101HXC	F	01/14/00
99695	INTERPOINT	9905	HYBRID	5962-9307201HXC	F	12/27/99
99889	Q-TECH	UNKN	HYBRID	QT6T10	F	10/14/99
99889	Q-TECH	UNKN	HYBRID	QT6T10	P	10/14/99
99787	ANALOG DEVICES	9807	MICROCIRCUIT	5962-8770204RA	P	10/12/99
99787	ANALOG DEVICES	9807	MICROCIRCUIT	5962-8770204RA	P	10/12/99
EC JOBS						
Job Number	Manufacturer	Date Code	Part Type	Part Number	Result	Date
00457	ELECTRO PLATE	UNKN	PWBOARD	1A26264-101 REV A	P	10/28/99
00458	PIONEER CIRCUITS	9941	PWBOARD	63-70048 REV G	F	10/25/99
00454	BF GOODRICH	391	PWBOARD	810945-1 REV A	P	10/25/99
00455	BF GOODRICH	378	PWBOARD	832485-1	P	10/25/99
00459	PIONEER CIRCUITS	9941	PWBOARD	63-70047 REV G	P	10/22/99
00453	SPEEDY CIRCUITS	9939	PWBOARD	INT DSP MEMORY REV B	P	10/22/99
00451	ELECTRO PLATE	9908	PWBOARD	1A26261-101 REV A	P	10/21/99
00417	SUN CIRCUITS INC	4099	PWBOARD	1A26379-101 REV A	P	10/21/99
00452	SOVEREIGN CIRCUITS	9934	PWBOARD	GD2036914	P	10/20/99
00446	SUN CIRCUITS INC	4099	PWBOARD	1A26391-101 REV A	P	10/20/99
00438	PRINTCA	UNKN	PWBOARD	PROPULSION MODULE	P	10/19/99
00444	TYCO ENGINEERED	499	PWBOARD	GD2025416-1 REV A	P	10/19/99
00445	TYCO ENGINEERED	499	PWBOARD	GD2025417-1 REV A	P	10/19/99
00437	ACTION COMPUTER	9934	PWBOARD	11006628-1 REV G	P	10/18/99
00443	CIMULEC	9917	PWBOARD	GYRO SUPPLY	P	10/18/99
00442	CIMULEC	9912	PWBOARD	HEATER MODULE	P	10/18/99
00431	PRINTCA	31754	PWBOARD	MTE PCB1	F	10/15/99
00447	SUN CIRCUITS INC	3899	PWBOARD	1A26328-101 REV A	F	10/15/99
00456	SUN CIRCUITS INC	1599	PWBOARD	2A07653 REV A	P	10/15/99
00450	ADVANCED QUICK	9939	PWBOARD	GD2027553	P	10/14/99
00449	TYCO ENGINEERED	6541	PWBOARD	GD2038640-1	P	10/14/99
00427	SPEEDY CIRCUITS	9934	PWBOARD	MUX2 REV C (AM2)	P	10/13/99
00448	TYCO ENGINEERED	6541	PWBOARD	GD2038639-1	P	10/13/99
00436	ACTION COMPUTER	9934	PWBOARD	11004500-1 REV G	P	10/12/99
00435	ADVANCED QUICK	3899	PWBOARD	186994-1	F	10/12/99
00418	PIONEER CIRCUITS	9936	PWBOARD	1028042	F	10/10/99
00424	SPEEDY CIRCUITS	9934	PWBOARD	MUX1 REV C (AM1)	P	10/08/99
00430	GRAPHIC RESEARCH	9921	PWBOARD	2A05726-101	P	10/08/99
00416	TYCO ENGINEERED	3999	PWBOARD	GD2036856-1	P	10/08/99
00412	COLONIAL CIRCUITS	9935	PWBOARD	GD2040545-1	F	10/07/99
00414	AMBITECH INC	9933	PWBOARD	8168581-1/-2/-3 REV A	P	10/07/99
00415	SAS CIRCUITS, INC.	3899	PWBOARD	XY DIGITIZER	F	10/07/99
00413	ADVANCED QUICK	3699	PWBOARD	GD2038634-1	P	10/07/99
00428	TYCO ENGINEERED	65416	PWBOARD	GD2040538-1	P	10/06/99
00429	TYCO ENGINEERED	65416	PWBOARD	GD2040537-1	P	10/06/99
00433	SOVEREIGN CIRCUITS	9937	PWBOARD	1641-002-001	P	10/06/99
00434	SOVEREIGN CIRCUITS	9937	PWBOARD	1641-002-002	P	10/06/99
00411	COLONIAL CIRCUITS	9935	PWBOARD	GD2040530-1	P	10/06/99
00432	PRINTCA	31537	PWBOARD	MTE PCB2	P	10/04/99
00420	PIONEER CIRCUITS	9938	PWBOARD	63-70049	P	10/04/99
00421	PIONEER CIRCUITS	9938	PWBOARD	63-70046	P	10/04/99
00410	SAS CIRCUITS, INC.	3499	PWBOARD	20323 REV A	P	10/04/99